Nanostructures Technology, Research and Applications

Academic and Research Staff
Prof. Karl Berggren, Dr. Rajesh Menon, Mark K. Mondol, Dr. Euclid Moon, Dr. Mark L. Schattenburg, Prof. Henry I. Smith

Visiting Scientists, Postdoctoral Associates and Research Affiliates
Prof. Maria Csete, Dr. Timothy Savas, Dr. Francesco Marsilli, Dr. Stephan A. Schulz, Dr. Sebastian Strobel

Graduate Students
Lorenzo Battistella (visiting), Bryan Cord, Jae-Byum Chang, Eric Dauler, Huigao Duan (visiting), Corey Fucetola, Charles Herder, Charles Holzwarth, Xiaolong Hu, Joshua Leu, Vitor Manfrinato, Adam McCaughan, Faraz Najafi (visiting), Tom O'Reilly, Amil Patel, Thomas Reisinger (visiting), Michael Snella, Jie Sun, Hsin-Yu Tsai, Lin Lee Cheong, Donald Winston, Joel Yang

Collaborators and NSL Users
Prof. Mark Baldo, Prof. George Barbastathis, Prof. Jacopo Buongiorno, Prof. Jesus DelAlamo, Prof. Silvija Gradecak, Prof. Vivek Goyal, Dr. Scott Hamilton, Prof. Erich Ippen, Prof. John Kasakian, Dr. Andrew J. Kerman, Prof. Franz Kaertner, Prof. Leslie Kolodziejski, Dr. Richard Molnar, Dr. Jagadeesh Moodera, Prof. Thomas Palacios, Dr. Jeffrey Peterson, Dr. Michael Postek, Prof. Rajeev Ram, Prof. Caroline Ross, Prof. Edwin L. Thomas, Prof. Carl Thompson, Dr. Andras Vladar, Dr. Stanley Williams, Dr. Wei Wu, Dr. Qiafeng Xia

Technical and Support Staff
James Daley, Alicia Akins

This chapter surveys the work going on in the NanoStructures Laboratory under the supervision of Profs. Henry I. Smith and Prof. Karl K. Berggren. The NanoStructures Laboratory includes the Scanning-Electron-Beam-Lithography Laboratory, which is discussed in a separate section below. The research ongoing includes work on nanofabrication and devices. The work supervised by Prof. Berggren additionally investigates the application and fabrication of devices using the foundations of quantum mechanics. We focus on: (1) superconductive devices and materials, single-photon detection and quantum computing; (2) nanofabrication methods; and (3) applications of nanofabrication to energy systems. Superconductive devices are among the most readily engineered examples of devices exhibiting quantum-mechanical effects. We therefore work with superconductive materials, including efforts in materials, processing, and analysis. Also, because quantum-mechanical effects are primarily observable at microscopic length scale, we develop and implement novel methods of nanofabrication. We take a multi-disciplinary approach to these topics, borrowing techniques from physics, electrical-engineering, computer science, chemistry, and materials science. The work supervised by Prof. Smith additionally investigates micro-and nanophotonic devices,and nanoscale lithographic methods.

NanoStructures Laboratory

Sponsors:
MIT Institute Facility under RLE

Project Staff:
Mark K. Mondol, James Daley, Prof. Karl Berggren, Dr. Mark Schattenburg, Prof. Henry I. Smith

In 2006, the Nanostructures Lab converted its fabrication facility in Room 39-477 into an Institute-wide service facility under the Research Laboratory of Electronics (RLE). This facility provides MIT and outside users with easily accessible Reactive Ion Etching (RIE), interferometric lithography, ebeam evaporation, resist spinning, wet bench developing, Scanning Electron

Microscopy (SEM), Atomic Force Microscopy (AFM) as well as a variety of associated lab tools and techniques required for nanofabrication. To maximize successful research access to tools is coupled with resident expertise and advice. The facility director is Prof. Karl Berggren. Prof. Hank Smith and Mark Schattenburg are associate directors. James Daley manages the day-to-day laboratory operations, provides training on the tools mentioned above, and student guidance on optimal nanofabrication techniques and strategies.

Projects that made use of the NSL facility during the past year included: relief templates for self assembly of block copolymers; ultra fast optical detectors; 1-D and 2-D photonic crystals; ring-resonator add/drop filters; optical-polarization splitter-rotator devices; magnetic-memory devices; quantum photodetectors; templates for nanoimprint lithography; photomasks for interferometric-spatial-phase-imaging alignment and gapping; 4-point contacts for measurements on nanotubes and nanowires; abosorbance modulation optical lithography and imaging; 3-D self folding structures; Si-Ge combined devices; arrays of Fresnel zone plates and thin resist exposure to investigate the ultimate limits of lithography. Use of the facility, by the MIT community, was widespread, there were: 20 Principal Investigators, 5 Departments, 4 Labs or Centers, 2 non-MIT entities and >80 distinct trained users over the last year.

Tools within the NSL Facility include: Zeiss 982 SEM, Digital Instruments AFM, 2 Leica optical microscopes, Plasma Therm RIE (Reactive Ion Etcher), March RIE, Samco ICP RIE, optical mask aligner, UV flood exposure, Gaerntner ellipsometer, Temescal ebeam evaporator, critical point dryer, sputtering system, ion miller, rapid thermal annealer, 3 wet benches, class 10,000 and class 100 cleanroom space and a Lloyd's mirror interferometic exposure system. There are also fume hoods, laminar flow hoods, hotplates, ovens, inspection microscopes, and a variety of hand tools and glassware required for nanofabrication. The NSL is housed in Building 39, which provides acid sinks, deionized water, dry N_2 and other building services, but has satellite laboratories with individual tools in buildings 26 and 38.

Scanning Electron Beam Lithography Laboratory

Sponsors:
MIT Institute Facility under RLE

Project Staff:
Mark K. Mondol, Prof. Henry I. Smith, Prof. Karl Berggren

In 2004, the Nanostructures Lab converted its scanning-electron-beam-lithography (SEBL) facility in Room 38-165 into an Institute-wide service facility under the Research Laboratory of Electronics (RLE). This facility provides MIT and outside users with easily accessible e-beam lithography, coupled with resident expertise and advice. The facility is managed by Mark Mondol who provides training on the e-beam tools, direct patterning service, and advice on optimal nanofabrication techniques and strategies. The NanoStructures Laboratory (NSL) and the Microsystems Technology Laboratories (MTL) have service facilities for spin coating of resists, resist development and other forms of processing.

Projects that made use of the SEBL facility during the past year included: patterned nanotube growth; relief templates for self assembly of block copolymers; point-contact devices; 1-D and 2-D photonic crystals; ring-resonator add/drop filters; optical-polarization splitter-rotator devices; magnetic-memory devices; quantum photodetectors; templates for nanoimprint lithography; photomasks for interferometric-spatial-phase-imaging alignment and gapping; 4-point contacts for measurements on nanotubes and nanowires; III-V compound T-gate HEMTs and arrays of Fresnel zone plates. Research in lithographic processing included salty development of HSQ (Hydrogen silsesquioxane) which demonstrated improved resolution and contrast. Use of the facility, by the MIT community, was widespread, there were: 27 Principal Investigators, 7

Departments, 8 Labs or Centers, 2 non-MIT entities and 75 distinct trained users over the last year.

Two SEBL tools are available. The Raith Turnkey 150 system is shown in Figure 1. Its electron-optical column is essentially identical to that of a Zeiss Gemini SEM, and provides a beam diameter as fine as 2 nm. 10 nm pitch, nested L patterns with linewidths of 5 nm have been written with the system, as illustrated in **Figure 2.**The Raith 150 includes a pattern generator and laser-interferometer-controlled stage with an integrated software package. Version 4.0 software now allows users to do automated field alignment to approximately ± 25nm. The system can operate from 1 to 30keV accelerating voltage. Wafers up to 150 mm can be loaded into the system. Typically, users are trained for 4 to 10 hours and then allowed to operate the tool on their own. The tool is available, for most users, 24 hours a day, 7 days a week.

Figure 3 is a photograph of the VS-26 system. This instrument was put together at MIT from two systems (VS-2A and VS-6) obtained as gifts from IBM in the mid 1990's. VS-26 has a minimum beam diameter of about 10 nm. It operates at a fixed accelerating voltage of 50keV. Conversion software has been developed which allows a CAD data file to be fractured and translated prior to exposure, additional software was developed to generate arbitrary arcs. Substrates up to 200 mm diameter can be exposed at linewidths down to ~30 nm. However, the area available for patterning is limited to 95x95 mm.

The Raith 150 is used in a program to develop spatial-phase-locked e-beam lithography, described elsewhere. The objectives of that program are to achieve sub-1 nm pattern-placement accuracy, and to reduce the cost and complexity of SEBL. In a conventional SEBL system costing several million dollars, pattern placement accuracy is typically much worse than 10 nm.
The SEBL facility encourages users with a variety of experience levels and requirements. Experienced users are able to carry out complex, multilevel aligned exposures on the Raith-150 tool. Less experienced users get hands-on instructions from facility staff, and guidance during the learning and initial fabrication stages.

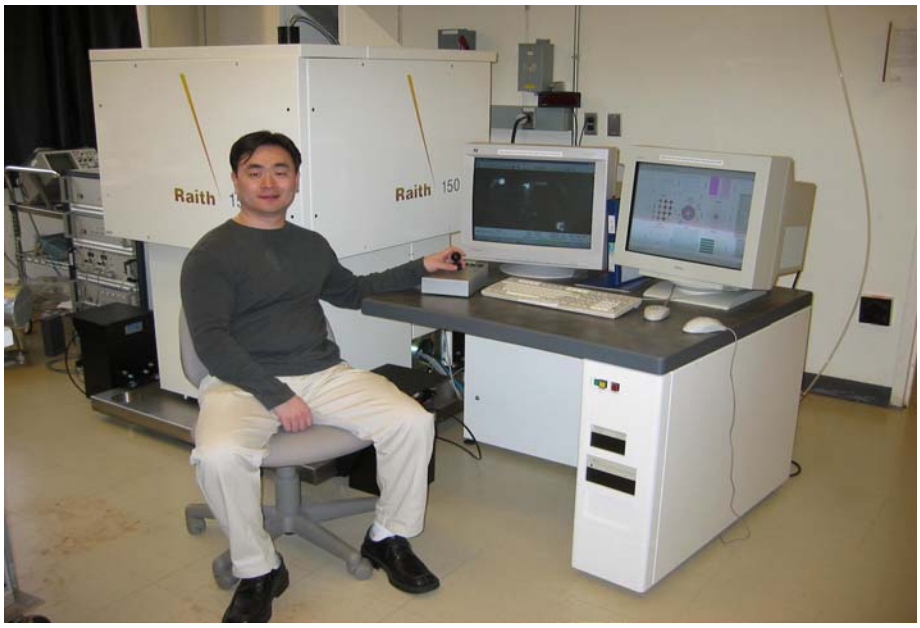

Figure 1. *The Raith-150 electron-beam lithography system. This tool provides sub-20-nm patterning resolution, and pattern-placement accuracy ~ 1nm via spatial phase locking. The operator is Dr. Feng Zhang.*

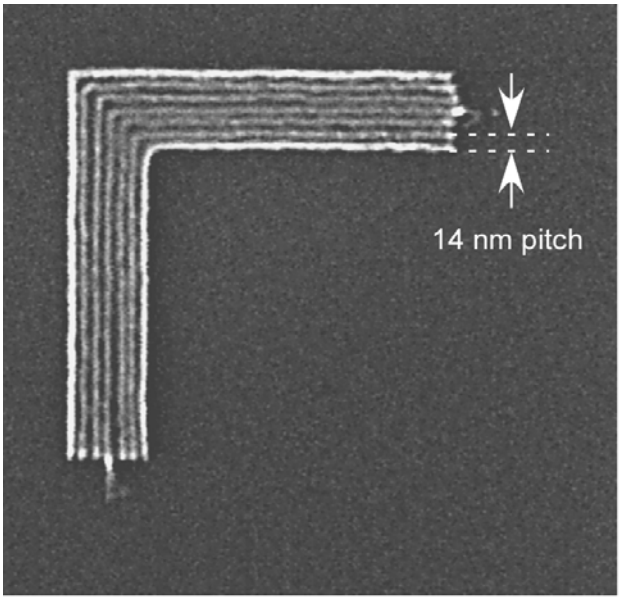

Figure 2: *Scanning-electron micrograph of exposed and developed HSQ illustrating the resolution of the Raith 150 SEBL system. (J. K. W. Yang and K. K. Berggren, "Using High-Contrast Salty Development of Hydrogen Silsesquioxane for Sub-10-nm-Half-Pitch Lithography," Journal of Vacuum Science & Technology B, submitted for publication (2007)*

Figure 3. *Photograph of the VS-26 scanning-electron-beam lithography system.*

Interference Lithography

Sponsors:
MIT Lincoln Lab Integrated Photonics Initiative

Project Staff:
Thomas B. O'Reilly and Prof. Henry I. Smith

Interference lithography (IL) is a means of rapidly creating periodic and quasi-periodic patterns that are spatially coherent over large areas. In principle, IL is a simple process where two mutually-coherent beams of light interfere to produce a standing wave pattern, which is recorded in a photosensitive material. In the most common configuration, two beams interfere forming a grating pattern, as shown in **Figure 1**. The spatial-period, *P*, of a grating produced using IL can be almost as small as half the wavelength of the interfering light (l). More complex patterns, such as square or hexagonal grids, can be formed by the use of multiple exposures or the use of more than two beams.

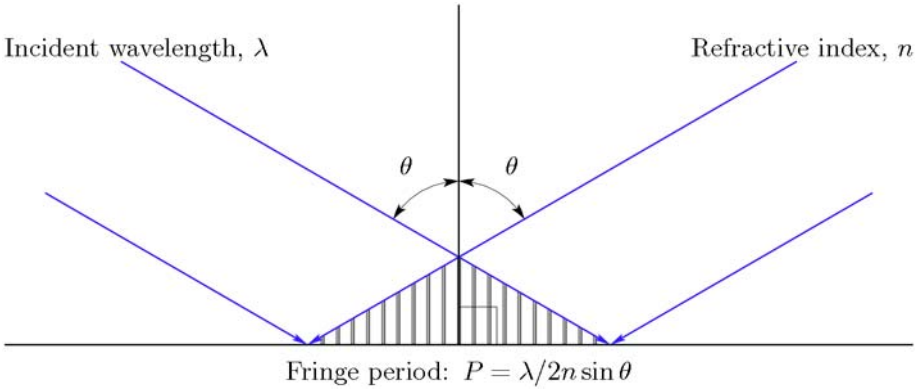

Figure 1. Interference geometry and resulting fringe periodicity in the most common configuration, two beams incident at equal angles to the surface.

The NanoStructures Lab has been developing IL systems and applications for over 30 years. We currently operate three different IL systems for a wide variety of applications, and have access to two more systems in the Space Nanotechnology Lab. The IL systems in the NSL have produced patterns with periods as small as 165 nm using a 325 nm Helium-Cadmium (HeCd) laser, and as small as 100 nm using a 193 nm Argon-Fluoride (ArF) laser.

One system, shown schematically in **Figure 2**, is configured as a Mach-Zehnder interferometer. It uses a HeCd laser with a wavelength of 325 nm. In this system, the beams are spatially filtered to ensure good spatial coherence. The absence of optical elements after the spatial filters eliminates distortion and coherent noise that might result from the use of collimating lenses, and produces very high quality fringe patterns. However, the use of spherical waves to form the interference pattern produces grating lines that are in fact hyperbolic rather than straight, with the periodicity varying by a few tenths of a nanometer (for a 200 nm period grating) over a 100 mm substrate. Although small, distortions of this scale can be significant, especially in metrological applications such as the fiducial grids for spatial-phase-locked electron-beam lithography. In addition to writing grids and gratings, this system has been used to measure grating distortion using a technique known as holographic phase-shifting interferometry (HPSI). With this technique, in-plane distortion of gratings and grids can be measured with a resolution of a few nanometers.

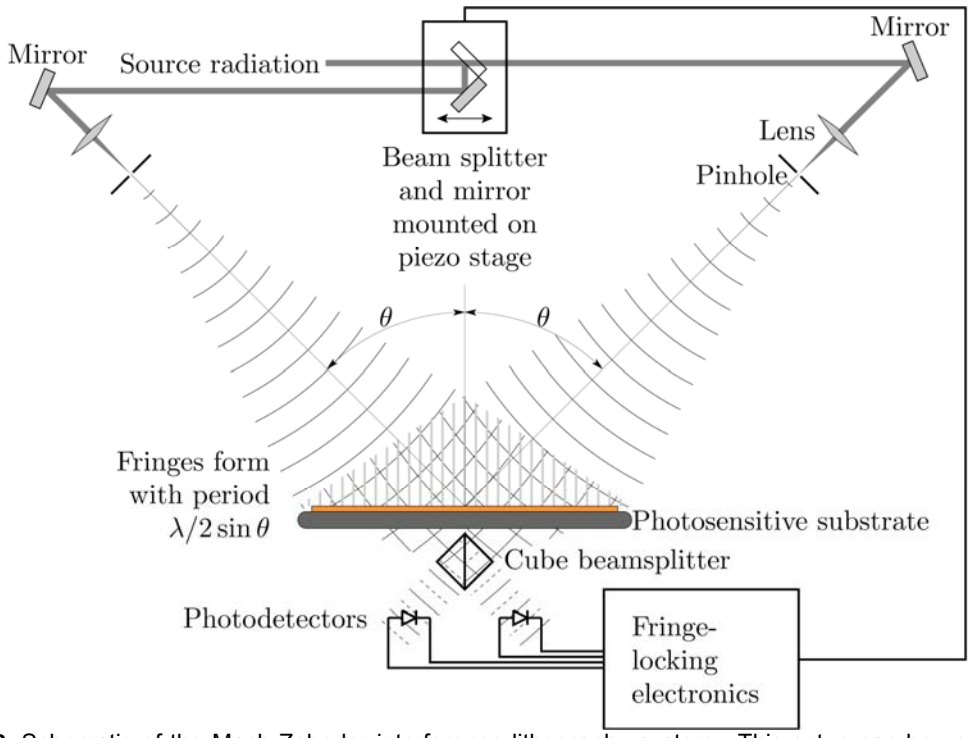

Figure 2. Schematic of the Mach-Zehnder interference lithography system. This setup can be used as an interference lithography system to write reference grids, as well as a holographic-phase-shifting interferometer to measure grid distortion.

The Lloyd's mirror interferometer, shown schematically in Figure 3, also uses a 325 nm HeCd laser. A single spatial filter is located 2 meters from the substrate. The substrate and a mirror perpendicular to it are illuminated such that part of the incoming light is reflected back to the substrate. Optically, the Lloyd's mirror system is similar to the Mach-Zehnder system, except that instead of light reaching the substrate from two separate spatial filters, it comes from one spatial filter and its mirror image. In addition to reducing the complexity of the optics required to form fringes, the fringes formed by the Lloyd's mirror system are stable enough that no fringe-locking system is required, making the system both simpler to operate and more robust. A major advantage of the Lloyd's mirror over a Mach-Zehnder style IL system is the ease with which the spatial period of the patterns produced can be changed. The substrate holder and mirror are mounted on a rotation stage. By rotating this stage, the interference angle can be quickly changed to write patterns with periods ranging from many microns down to about 165 nm. In comparison, changing the period of a Mach-Zehnder system requires considerable work to realign numerous optical elements.

The ease-of-use and flexibility of the Lloyd's mirror make it possible for a large number of researchers to use the system to produce periodic patterns for their own research, without needing to become experts in IL or spend a lot of time configuring the system for their needs. The Lloyd's mirror has been used for such diverse research projects as grids with different periods in the two directions for patterned magnetic media and MRAM (magnetic random access memory) devices, alignment templates for organic crystals, semiconductor quantum dots, and patterning for studies of templated self assembly of block copolymers, metal particles and nanowires. Distributed feedback (DFB) structures for quantum dot lasers and photonic bandgap devices have also been made using the Lloyd's mirror system. In addition, the system has been used to develop new methods of characterizing photoresist performance.

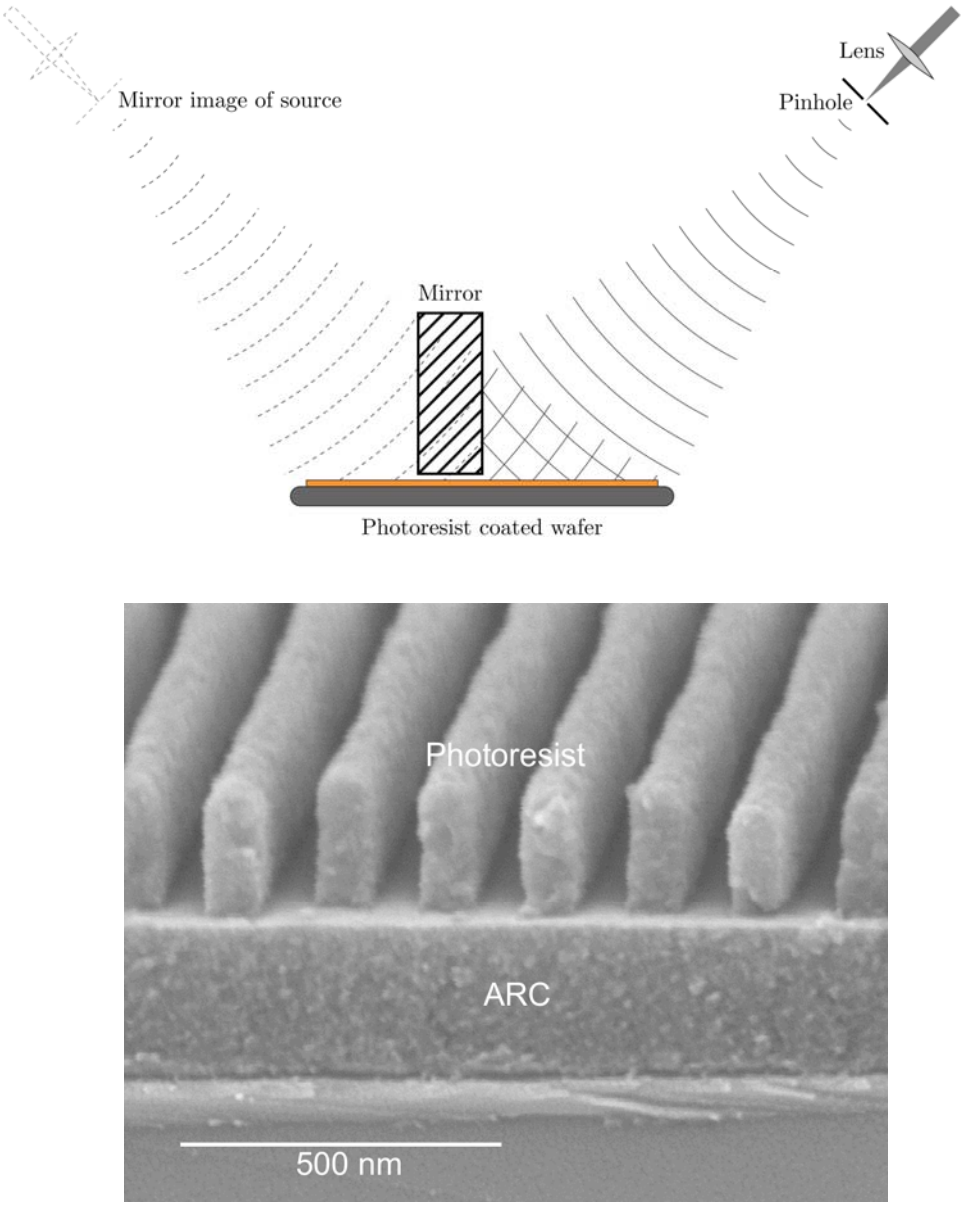

Figure 3 Schematic of a Lloyd's mirror interferometer. The substrate and mirror are fixed at a 90˚ angle to one another, and centered in a single incident beam. Rotating the substrate/mirror assembly varies the spatial-period of the exposed grating. The micrograph shows a grating with a 165 nm period exposed using the Lloyd's mirror.

We also operate an achromatic interference lithography system (AIL), to write patterns with spatial periods of 100 nm using light from a 193 nm ArF excimer laser. The AIL, shown schematically in Figure 4, is a grating interferometer configured in such a way that the contrast of the grating image formed is largely independent of the spatial and temporal coherence of the source, allowing large-area gratings to be written with a source that has limited temporal and spatial coherence. In this configuration, the spatial period of the exposed grating is dependent only on the period of the parent gratings, regardless of the wavelength and temporal coherence of the source. Thus, gratings and grids produced with this tool are extremely repeatable. Figure 4 also shows a 100 nm-period grid of 13 nm-diameter posts etched into silicon, produced with achromatic interferometric lithography (AIL) and a sequence of etching steps. Applications of AIL

include patterned magnetic media, free-standing gratings for atom-beam interferometry, and patterns for templated self-assembly.

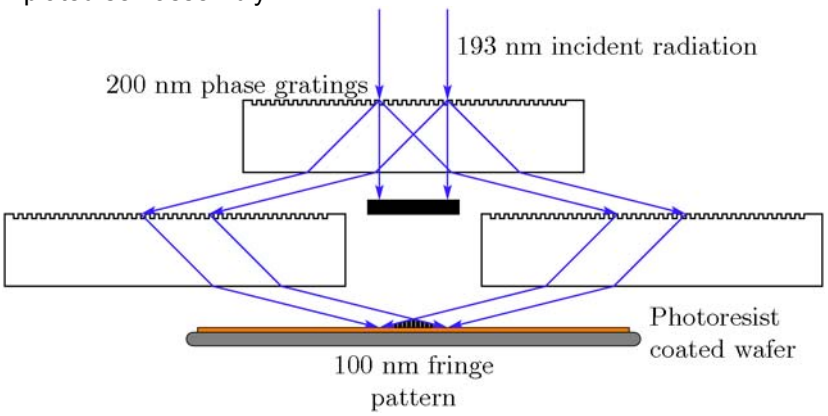

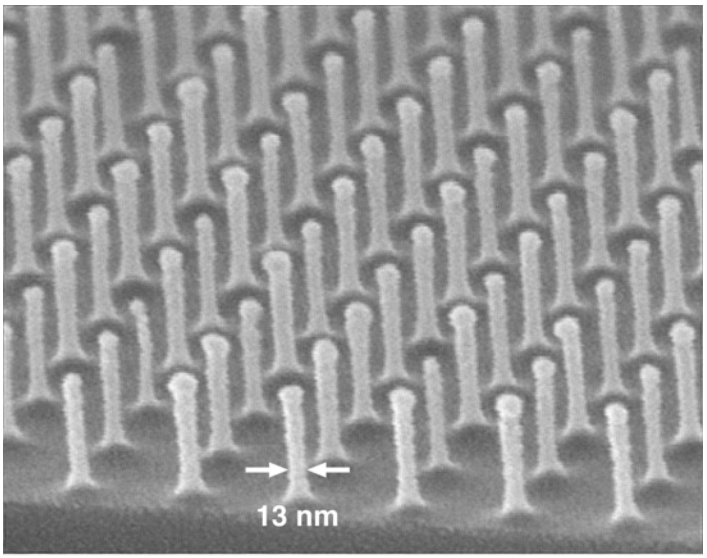

100nm-period posts in Si

Figure 4. (Top) Achromatic interferometric lithography (AIL) configuration used to produce 100 nm-period gratings and grids. (Bottom) Scanning electron micrograph of a 100 nm-period grid, exposed in PMMA on top of an antireflection coating, and transferred into silicon by reactive ion etching and $Si0_2$ etching.

Two additional systems are operated in conjunction with the Space Nanotechnology Lab (SNL). The first employs the Mach-Zehnder configuration, but is specially designed for high stability and repeatability. It is capable of producing metrological-quality gratings and grids up to 100 mm in diameter at spatial periods down to 200 nm. The most notable applications for gratings produced with this system is the Chandra x-ray astronomy satellite launched in August of 1999 which included hundreds of matched, high-precision gratings in thick gold for high contrast at x-ray wavelengths. SNL also operates a more advanced system called the NanoRuler, which is capable of making nearly perfect gratings over substrates up to 300 mm diameter using scanning-beam interference lithography.

References:
[1] Thomas B. O'Reilly and Henry I. Smith, "Photoresist characterization using double exposures with interference lithography," J. Vac. Sci. Technol. B, 26, 128 (2008).
[2] Thomas B. O'Reilly and Henry I. Smith, "Linewidth uniformity in Lloyd's mirror interference lithography systems," J. Vac. Sci. Technol. B, 26, 2131 (2008).

Sub-wavelength interference lithography with absorbance modulation

Sponsors:
MIT Lincoln Lab Integrated Photonics Initiative

Project Staff:
Thomas B. O'Reilly, Dr. Rajesh Menon, and Prof. Henry I. Smith

In the simplest type of interference lithography (IL) system, two mutually coherent beams of light interfere to form a periodic standing wave pattern that can be recorded on a photosensitive substrate. The minimum period of the pattern that can be produced is restricted to half the wavelength of the light being used. While shorter wavelength sources are available, the properties of short wavelength lasers are not always suitable for use in interference lithography. As a result, there is great interest in finding ways to write patterns with periods below the diffraction limit, so that fine-pitch patterns can be written over large areas with sources that are easy to work with. We are pursuing an approach to patterning below the diffraction limit by combining a dual-wavelength IL (DWIL) system and absorbance-modulation technology [1].

In absorbance-modulation optical lithography (AMOL), an absorbance-modulation layer (AML), is placed on top of the photoresist layer. The absorbance-modulation layer is a polymer film containing photochromic molecules that can be switched between two isomeric states using different wavelengths of light. An example of such a material is bis(bithienylethene) (BTE) which has two forms, as shown in Fig. 1.

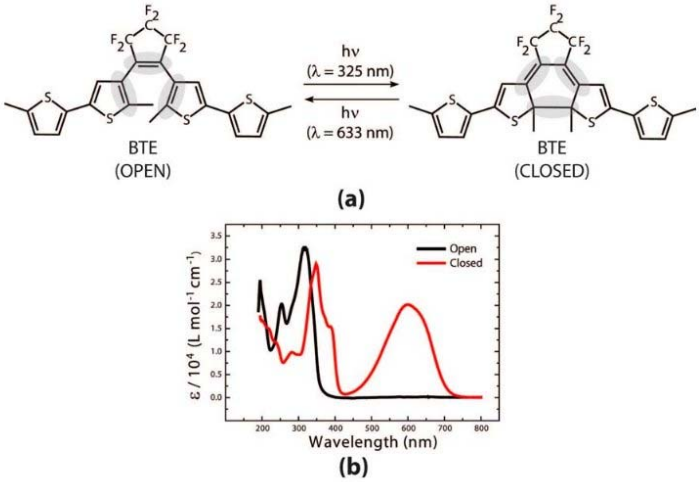

Figure 1: Molecular structure of the open and closed states of BTE. Exposure to UV wavelengths cause BTE to switch to the closed state, while exposure to longer wavelengths, (red light for example) causes BTE to switch to the open state.

As can be seen in the absorbance spectra for BTE in Fig. 1, exposure to UV wavelengths switches BTE to the closed form, which is more transparent to UV light around 300-350 nm than the open form. In contrast, exposure to red wavelengths switches BTE to the open form, which is less transparent to UV light. If an AML containing BTE is simultaneously exposed to standing

waves in both UV and red wavelengths, as shown in Fig. 2, it is possible to set up dynamic competition between the open and closed states, forming regions in the AML, with sizes much smaller than the wavelength, that are transparent to UV light. These regions effectively serve as subwavelength apertures in the AML through which the photoresist is exposed by the UV wavelength.

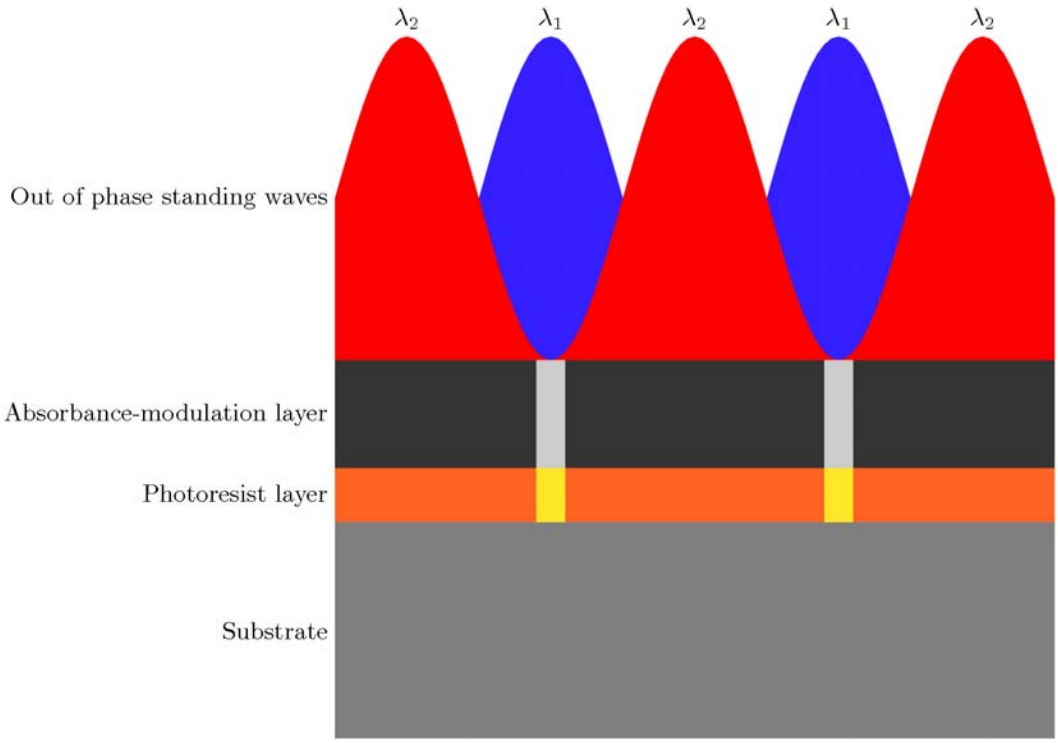

Figure 2: Schematic of the interaction of red and UV (shown in blue) wavelengths with an absorbance modulation layer. Out-of-phase standing waves formed by the two wavelengths result in the formation of narrow regions at the null of the red standing wave that are transparent to the UV light which serves to expose the photoresist. The AML narrows the width of the exposed regions compared to what would be possible with conventional IL exposures.

Since the states of the molecules in the AML are reversible, it is possible to shift the sets of fringes on the substrate, forming a new set of subwavelength apertures, and exposing a new set of lines in the resist. In effect, each exposure divides the spatial period of the original fringes, reducing the pitch of the final pattern. For example, if the initial spatial period were 400 nm, four exposures could be performed, shifting the fringes by 90 degrees after each exposure, to reduce the final period of the pattern to 100 nm. Ultimately, the extent to which the period can be divided will be limited by the performance of both the absorbance modulation layer and the photoresist, making a system to test and characterize AMOL materials an important tool.

We are presently developing a DWIL system to be used both to test materials for use with AMOL and to provide a means of achieving sub-100nm period interference lithography with a relatively simple system and relatively long wavelengths. The planned system, shown schematically in Fig. 3, will form two standing waves, one using 351 nm light from an argon ion laser and a second from a longer wavelength, red laser. In essence, the system consists of two independent Mach-Zehnder style IL systems, simultaneously illuminating the same substrate.

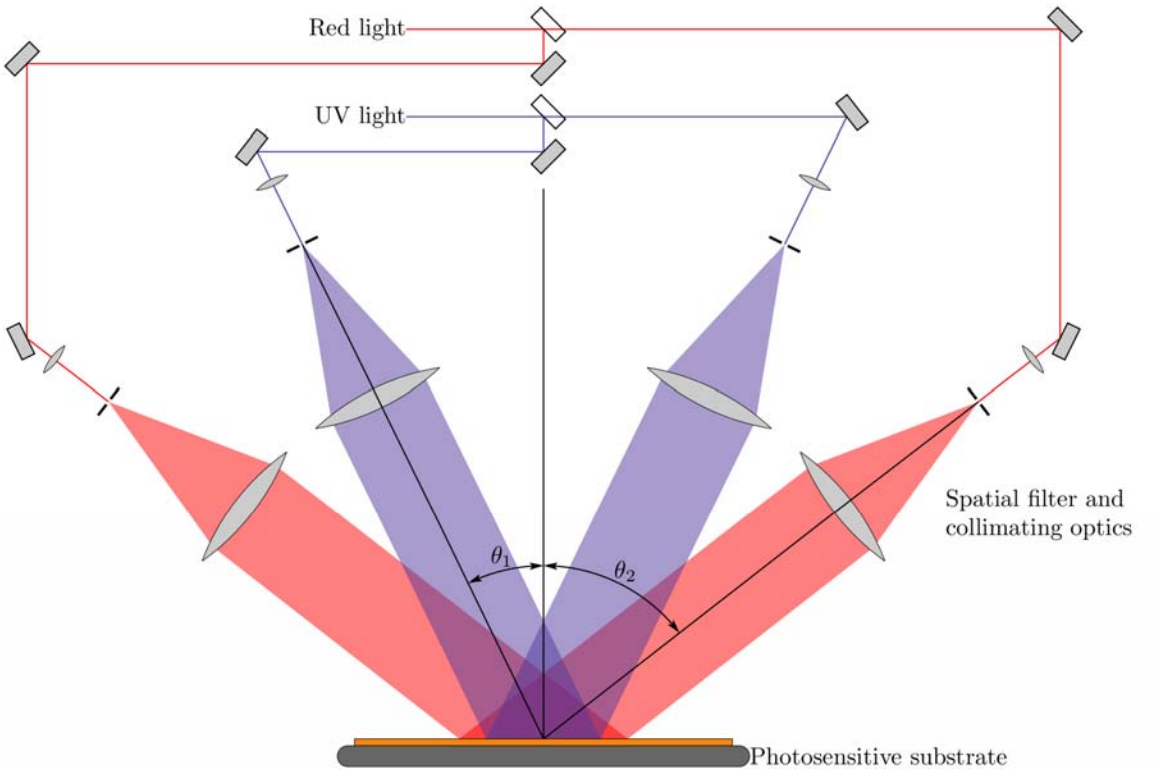

Figure 3: Schematic of dual-wavelength IL system. Beams of two different wavelengths are split, expanded and collimated to simultaneously form standing waves of the same period in two different wavelengths.

The chief challenge of a DWIL system is to match the period of the two standing waves and control their relative phase. This will be accomplished through the use of a reference grating placed next to the exposure area, with a period twice the period of the fringes being formed by the DWIL system. When the incident UV and red beams are properly aligned, light from each of the four incident beams is diffracted in a direction normal to the surface of the reference grating, as shown in Fig. 4. Interference between the two normally diffracted orders of each wavelength forms a pattern that can be used both to ensure that the periods of the two fringe patterns match and to control the phase of the standing wave pattern relative to the phase of the reference grating.

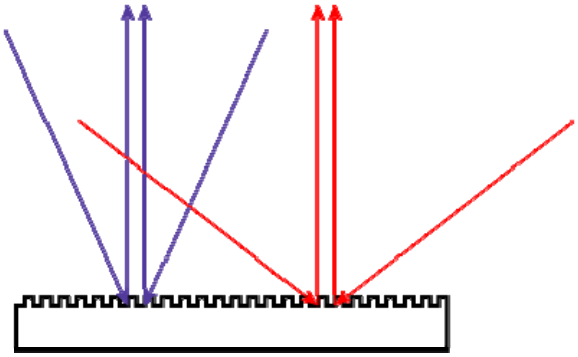

Figure 4: Schematic of the reference grating, which is mounted next to the exposure area. The period of the reference grating is twice the period of the fringes being written. When the incident beams are properly aligned, light from each of the wavelengths diffracts in a direction normal to the surface of the reference grating.

References:

[1] Rajesh Menon and Henry I. Smith, "Absorbance-modulation optical lithography," J. Opt. Soc. Am. A **23**, 2290-2294 (2006).

Ensuring Precision of Overlay in Photonic-Crystal Lithography

Sponsors:

AFOSR and MIT Institute for Soldier Nanotechnologies

Project Staff:

Corey P. Fucetola, Amil A. Patel, Dr. Euclid E. Moon and Prof. Henry I. Smith

This project aims to develop a new approach to constructing 3-dimensional systems. In brief, the 3-D structure is formed by the stacking of membranes. This stacking approach enables one to pattern the membranes prior to assembly, thereby achieving a highly complex 3-D system using only 2-D patterning technology, which is already well-developed.

Our initial objective is the fabrication of 3-D photonic crystals, in Si and SiNx, with devices located in the photonic-crystal interior. Applications of 3-D photonic crystal devices include passive reflectors, lossless optical waveguides, extremely high-Q optical resonators, suppression of spontaneous emission, single-photon sources, negative refraction, slow light, chemical sensing with single-molecule sensitivity, quantum information processing, and extremely compact femto-second lasers that can be integrated with CMOS electronics. All of these applications benefit from the 3-D confinement only possible through 3-D photonic crystals.

The 3-D photonic crystal consists primarily of periodic structures. The particular 3-D photonic crystal of interest, a passive reflector, can be made from stacked membranes, each consisting of a 4-fold symmetric array of holes and a 4-fold array of posts, shifted slightly from the holes, as depicted in Fig. 1. The placement of the array of posts with respect to the holes is such that any post falls between only two holes. Then, upon stacking the membranes, the final periodicity in the third dimension is formed between the overlaid post-hole-post-hole positions.

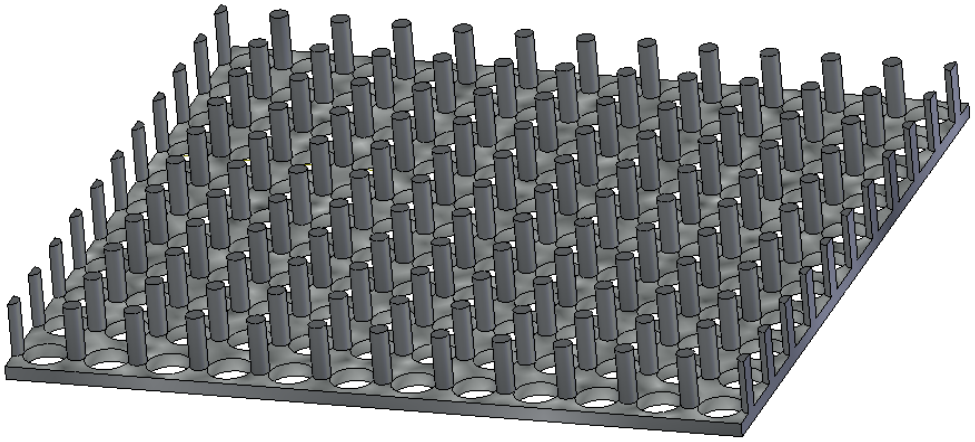

Figure 1: Two-dimensional square geometry photonic crystal membrane design consisting of two feature layers. The bottom layer is a layer of holes 145nm thick and the top layer of posts is 585nm thick. The periodicity in the x and y directions is 660nm for both layers. Any given post is between two holes, not four. This structure is designed to reflect in-plane 1.55μm light regardless of polarization.

Interference Lithography (IL) can make a 4-fold symmetric pattern but conventional IL cannot easily overlay two 4-fold symmetric patterns. Figure 2 shows a 4-fold pattern of holes transferred into a $1mm^2$ silicon membrane made using conventional IL. Generating the second 4-fold pattern of posts and overlaying it onto the patterned (pre-released) membrane is necessary to create the structure shown in Figure 1. However, generation of a second periodic pattern using conventional IL tools introduces variations in the pitch, duty-cycle and symmetry that will adversely affect the quality of the overlay. The pitch depends on the interfering angle and at 660nm an error of 11arc-seconds corresponds to a 1% change in pitch. Though control over the duty cycle is possible with conventional IL, making a 4-fold symmetric pattern requires 2 exposures, wherein the second exposure the substrate is rotated by 90°. If the substrate is rotated by 90 degrees and 11 arc-seconds in the second exposure, then the grid produced will not be orthogonal and the error in the grid pattern in will be 2.1nm after one period. These considerations require another approach; we call it Coherent-diffraction Lithography (CDL) [2].

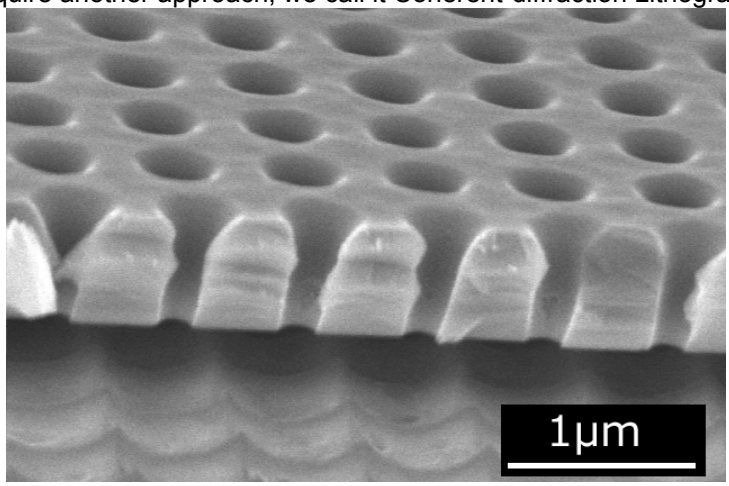

Figure 2: Fabricated Hole Layer: the silicon device layer of an soi wafer is shown after it was released from the buried oxide layer. The aspect ratio of the membrane's lateral extent to thickness for this membrane was greater than 1500.

Figure 3 shows the Coherent-diffraction Lithography tool and schematic. CDL was implemented to accommodate the need for repeatable periodic pattern replication. Our tool incorporates Interferometric Spatial-phase Imaging (ISPI) for multilayer alignment. CDL uses the Talbot effect to replicate the periodic pattern on a mask. This effect arises from the superposition of diffracted beams emanating from a grating: downstream of the grating the diffracted orders recombine into a periodic intensity pattern at planes parallel to the grating, called Talbot planes. ISPI [1] allows precise 6-axis closed-loop positioning between the mask and substrate by imaging back-diffracted and reflected light to determine the relative position between the mask and substrate. Combined, the Talbot effect and ISPI is ideal for photonic-crystal lithography.

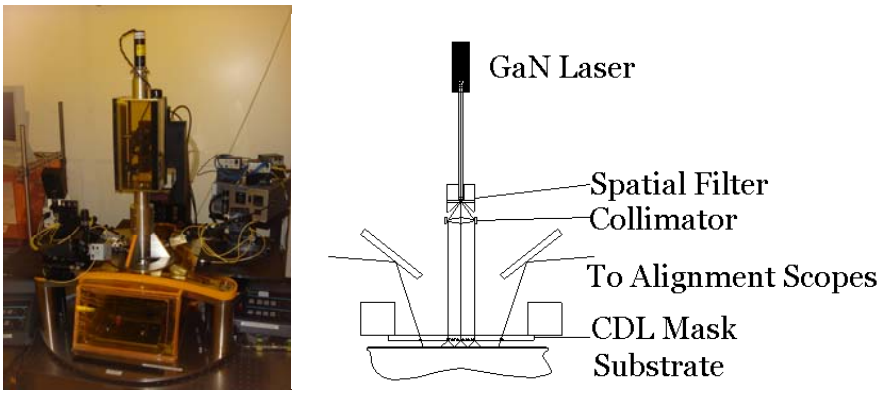

Figure 3: ISPI & CDL: Apparatus, System Schematic. Light from the GaN laser is spatially filtered prior to irradiating the CDL Mask. Combined with the ISPI alignment scheme, the filtered light passes through the mask and interferes on the substrate.

If a photoresist-coated substrate is placed at one of the Talbot planes it will record an intensity pattern with exactly the same period and spatial phase as the mask. This suggests the CDL approach, which circumvents the issues facing conventional IL, is the ideal approach to patterning the structures depicted in Figure 1. Two patterns generated at the same gap using the same mask will have the same period and phase. Shifting the second pattern by half the period in a direction parallel to a grid vector allows the features of the second pattern to correctly overlay onto the features of the first pattern. Patterning the substrate requires the capability to measure and control both the separation between, and lateral translation of, the photosensitive substrate relative to the mask.

The n^{th} Talbot plane, located a distance $Z_{n,m}$ downstream of the grating mask, arises from the interference pattern generated by diffracting light. A rigorous formulation of the n^{th} Talbot distance for the m^{th} order, $Z_{n,m}$, was derived. Noting that the standing-wave intensity pattern generated from two diffracted orders, of wavelength λ, has a spatial frequency in the **z**-direction, $\kappa_{m,\mathbf{z}}$, that is captured by the difference between the two spatial frequencies ($k_{m=0,\mathbf{z}}$ and $k_{m=1,\mathbf{z}}$) of the original diffracted orders, and that the Talbot distance in the **z**-direction is inversely related to its spatial frequency gives:

$$\therefore Z_{1,m} = 1\lambda\left(1-\cos\left(\theta_m\right)\right)^{-1} \tag{1}$$

The set of diffraction angles, θ_m, are constrained by the periodicity, p, of the diffraction grating and normally-incident wavelength, λ, and so the n^{th} Talbot distance can be described by:

$$\therefore Z_{n,m} = n\lambda\left(1-\sqrt{1-\left(m\lambda/p\right)^2}\right)^{-1} \tag{2}$$

This analysis could be carried out for the interference between any of the diffracted orders produced by the mask. Moreover, this analysis suggests that the mask must be carefully

designed because Talbot distances depend on the diffracted orders produced by the mask. However if the diffracted orders are restricted to m= -1,0 and 1 then the Talbot distances are well-defined, with $Z_{1,1}$=1.92μm.

Figure 4 shows the first two Talbot planes and downstream interference pattern resulting from light that is diffracted by a grating mask. The diffracted light is separated into diffracted orders following the grating equation:

$$-1 \le \sin\theta_m = \frac{m\lambda}{p} \le 1$$

For a wavelength of 405nm and our design period of 660nm the propagating diffracted orders are restricted to m=0, 1 and -1 and $\theta_{\pm 1}$= ±37.85° measured from propagation direction of the 0th order. The interference pattern is periodic in both directions and, parallel to the mask at Talbot planes, the mask is self-imaged.

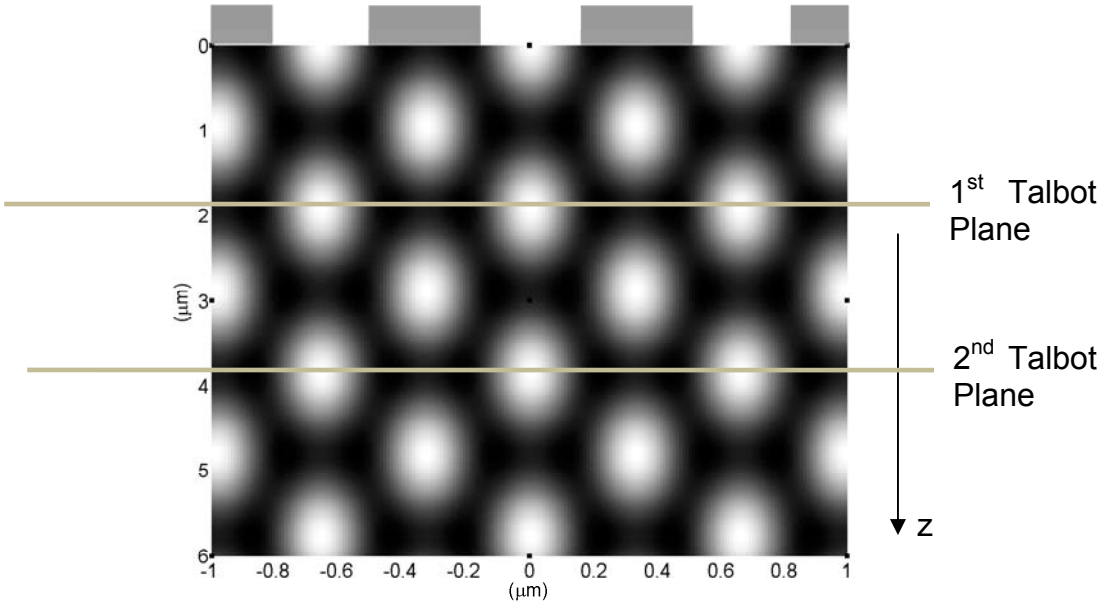

Figure 4: A plane wave is distributed by the mask into diffracted orders, which propagate at angles relative to the **z**-direction of the incident light. For a 660nm period and 405nm wavelength the first Talbot plane is at $Z_{1,1}$=1.92μm. At $Z_{1,1}$ the orders interfere forming an intensity pattern with the same periodicity and spatial phase as that of the mask.

Figure 5 shows a diffraction grating printed in photoresist at a parallel gap of 2μm using a CDL mask having only the m=-1, 0 and 1 orders. The gap was measured and controlled using the interference of red-light diffracted from ISPI marks on the mask surface. The red light irradiating the ISPI mark is both back-diffracted toward a detector and forward-diffracted to reflect off the substrate. The reflection then forward-diffracts again through the mark toward the detector and interferes with the back-diffracted beam. The fringe pattern formed on the detector contains information about the phase difference between each interfering beam and, hence, information about the distance between the mask and substrate [1]. Measuring and controlling the separation at three locations parallelizes the mask and substrate and allows CDL to take advantage of the Talbot effect.

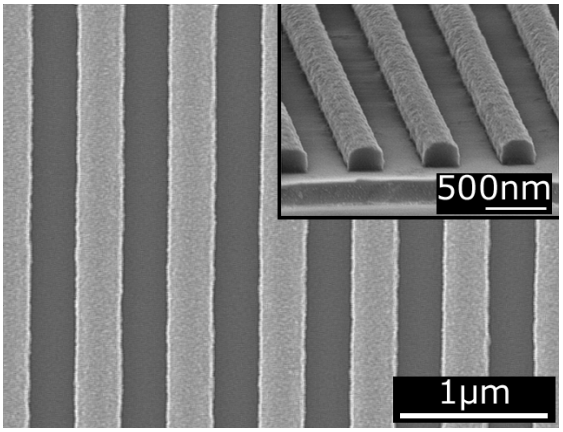

Figure 5: Top view and cross-sectional view of a grating produced in a positive photoresist using CDL at a gap of 2μm. The exposure dose was 57.5mJ/cm^2.

If the substrate and mask are configured at a slight wedge to each other then the intensity pattern printed into the photoresist will slowly vary through several Talbot planes. The left side of figure 6 shows an image of a wedge exposure using a grating mask and the right side shows an image of a wedge exposure using a grid mask (a 2-D square pattern of holes in SiN_x). The exposure using the grating mask confirms a Talbot distance of ~10*λ/2=2μm because the fringes along the bottom left each correspond to an increase in gap of a half-wavelength.

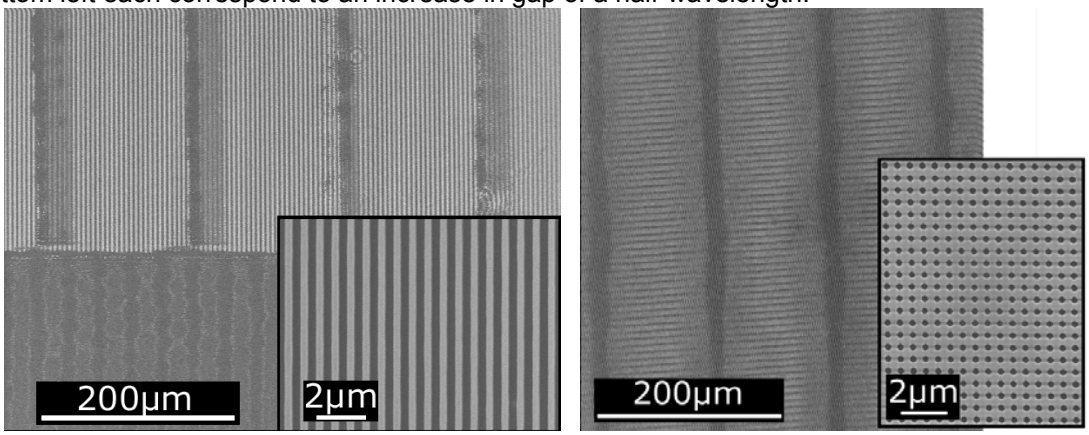

Figure 6: Wedge exposures: The mask to substrate gap is changing along the horizontal direction. (left) Resultant patterns from a grating mask with 600nm pitch and a 125nm tall relief structure. (right) Resultant patterns from a Grid mask (of holes) with 600nm pitch in both the X and Y direction and a 300nm tall relief structure. In each, the inset depicts the self-imaged pattern.

The results shown in figures 5 and 6 confirm that the Talbot effect can be used to self-image both 1-D and 2-D periodic structures. The next step in realizing the structure shown in figure 1 is fabricating the lateral-translation ISPI marks on the CDL mask. With these marks, we believe that the overlay process required to create the single 2-D TEM photonic crystal will be possible.

References

[1] Euclid E. Moon, Lynn Chen, Patrick N. Everett, Mark K. Mondol, and Henry I. Smith, "Interferometric-spatial-phase imaging for six-axis mask control," J. Vac. Sci. Technol. B **21**(6), Nov/Dec 2003

[2] Christel Zanke, Minghao Qi, and Henry I. Smith "Large-area patterning for photonic crystals via coherent diffraction lithography," J. Vac. Sci. Technol. B **22**(6), Nov/Dec 2004

Spatial-Phase-Locked Electron-Beam Lithography

Sponsors:
National Science Foundation

Project Staff:
Dr. Euclid E. Moon, Lin Lee Cheong, Prof. Henry I. Smith, Prof. J. Todd Hastings (U. Kentucky)

Our research in spatial-phase-locked electron-beam lithography (SPLEBL) is conducted in collaboration with the University of Kentucky. It is aimed at reducing pattern-placement errors in scanning electron-beam-lithography systems to the sub-1 nm level. Such high precision is essential for certain applications in photonics and nanoscale science and engineering. SPLEBL is currently the only approach capable of achieving such pattern-placement accuracy. As shown in Fig. 1, SPLEBL uses a periodic signal, derived from the interaction of the scanning e-beam with a fiducial grid placed directly on the substrate, to continuously track the position of the beam while patterns are being written. Any deviation of the beam from its intended location on the substrate is sensed, and corrections are fed back to the beam-control electronics to cancel beam-position errors. In this manner, the locations of patterns are directly registered to the fiducial grid on the substrate.

The research effort at MIT is now focused on developing the materials and processes for producing the fiducial grid, with the objectives of: maximizing the signal-to-noise of the secondary-electron signal derived from the grid; minimizing electron scattering from the grid, which would be deleterious to precision lithography; maximizing the area and absolute accuracy of the grid; and minimizing the cost and inconvenience of producing the grid on substrates of interest.

The current approach derives the modulation of the secondary-electron signal purely from the topography of the grid, as depicted in Fig. 2. The fabrication is exceedingly simple: the electron beam resist is covered with a grid in a G-line resist, and a few-nanometer coating of metal. Since most e-beam resists are not sensitive in the visible and near-UV, and since most e-beam resists are dissolved in different solvents than are G-line resists, we are able to use the two resists independently. We expose the G-line resist to interference lithography (using a Mach-Zender interferometer or coherent-diffraction lithography) and develop it to form the fiducial pattern. We then uniformly coat the grid with a metal such as Al, providing an enhancement of secondary-electron yield at the vertical sidewalls. An example of a grating made in this manner is shown in Fig. 3. When an electron beam scans across such a pattern there are spikes in the secondary electron emission from the sides of the vertical walls, due to enhanced electron escape probability along the sidewalls, as illustrated in the data in Fig. 4. The metal and photoresist are stripped before the e-beam resist is developed.

Further research will include selection of the grid thickness, metal thickness, and metal type to optimize the signal-to-noise ratio. In addition, if there is incompatibility of solvents between the G-line resist and the e-beam resist we can add a thin film of water-soluble poly-vinyl alcohol between the electron-beam resist and the G-line resist. Finally, the shape of the grid sidewalls can be tailored to optimize the secondary-electron signal in the fundamental grid frequency, and minimize the higher spatial frequency lobes observed in Fig. 4.

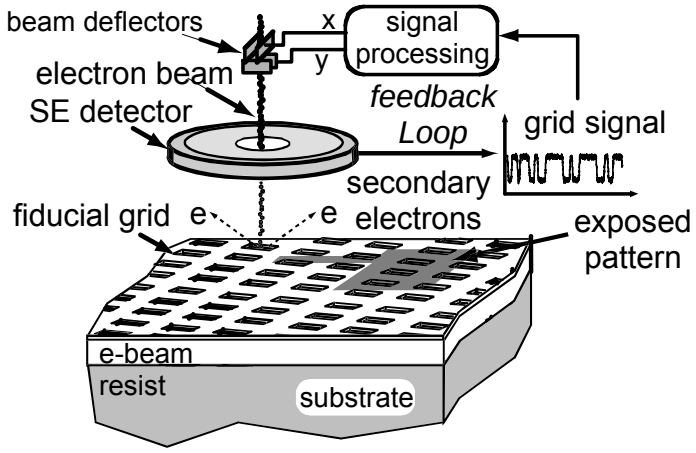

Figure 1: Schematic of the global-fiducial-grid mode of spatial-phase-locked electron-beam lithography. The periodic signal detected from the fiducial grid, which includes both X and Y components, is used to measure placement error, and a correction signal is fed back to the beam-deflection system.

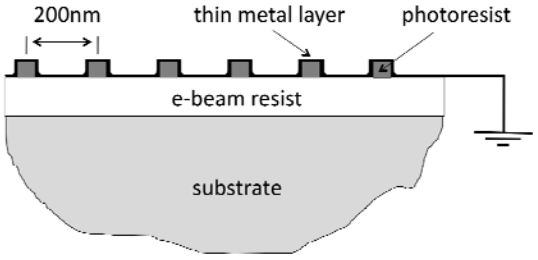

Figure 2: Cross-sectional schematic of a simple grid structure with a few-nanometer metal coating. The photoresist thickness should be small enough to be non-perturbative to the electron-beam lithography.

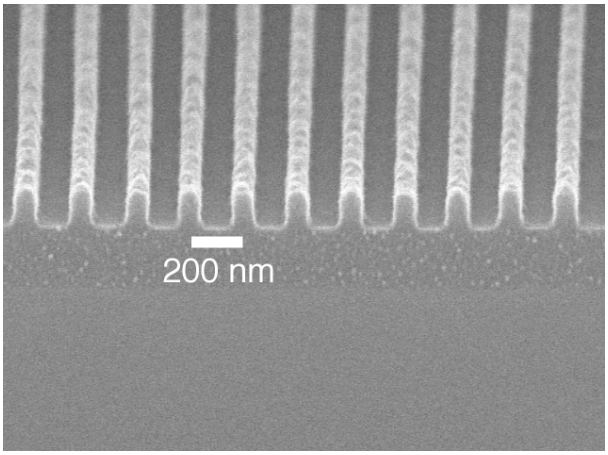

Figure 3: SEM micrograph of a fiducial grating in PFI-88 photoresist. The resist is covered conformally with a 3 nm layer of Au/Pd.

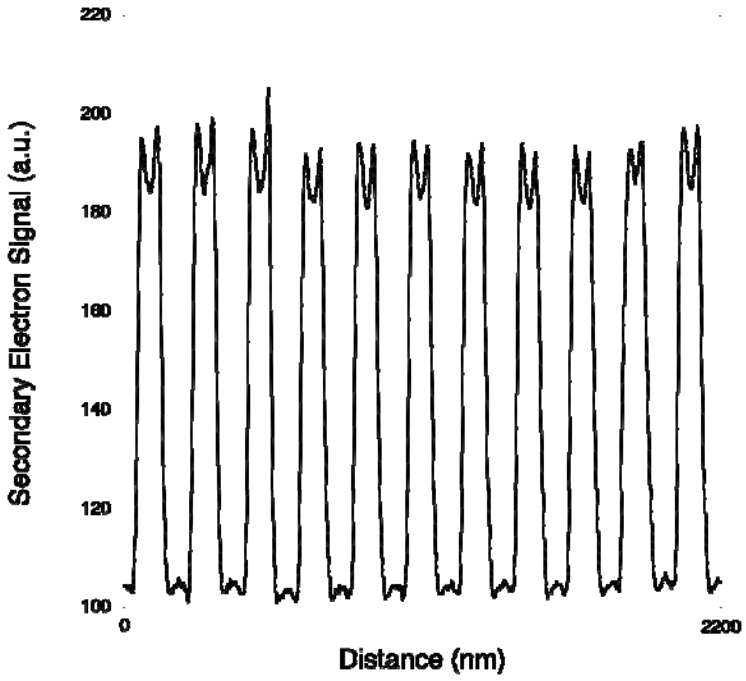

Figure 4: Plot of the secondary-electron yield in the grating of Fig. 3, averaged along the grating lines.

References:

[1] J.T. Hastings, F. Zhang, and H.I. Smith, "Nanometer-level stitching in raster-scanning e-beam lithography using spatial-phase locking," *J. Vac. Sci. Technol.* B, **21**, 2650 (2003).

[2] F. Zhang, H.I. Smith and J.F. Dai, "Fabrication of high-secondary-electron-yield grids for spatial-phase-locked electron-beam lithography," *J. Vac. Sci. Technol.* B, **23**, 3061 (2005).

[3] A.V. Krishnamurthy, R.V. Namepalli, and J.T. Hastings, "Subpixel alignment for scanning-beam lithography using one-dimensional, phase-based mark detection," *J. Vac. Sci. Technol.* B, **23**, 3037 (2005).

[4] J.T. Hastings, "Real-time determination of electron-beam probe shape using an *in situ* fiducial grid," *J. Vac. Sci. Technol.* B, **24**, 2875 (2006).

[5] Y. Yang and J.T. Hastings, "Real-time spatial-phase locking for vector-scan electron beam lithography," *J. Vac. Sci. Technol.* B, **25**, 2072 (2007).

[6] C.B. Samantaray and J.T. Hastings, "Self-assembled monolayer fiducial grids for spatial-phase-locked electron-beam lithography," *J. Vac. Sci. Technol.* B, **26**, 2351 (2008).

[7] Y. Yang and J.T. Hastings, "Field-programmable gate array implementation of real-time spatial-phase locking for electron-beam lithography," *J. Vac. Sci. Technol.* B, **26**, 2316 (2008).

[8] C.B. Samantaray and J.T. Hastings, "The effect of thin metal overlayers on the electron beam exposure of polymethyl methacrylate," *J. Vac. Sci. Technol.* B, **26**, 2300 (2008).

Fabrication of Free-Standing Silicon-Nitride Zoneplates for Neutral-Helium Microscopy Using Segmented-Spatial-Phase-Locked Electron-Beam Lithography

Sponsors:
Bergen Research Foundation

Project Staff:
Thomas. Reisinger, Corey Fucetola, Thomas B. O'Reilly, Lin L. Cheong, Prof. Henry I. Smith and Prof. B. Holst

Neutral helium microscopy is a relatively new technique which employs a focussed supersonic expansion helium beam (~50meV) to image a sample in scanning mode. It potentially offers significant advantages. Firstly, the atoms are neutral, which means that insulating surfaces can be imaged without prior coating. Furthermore, the energy of the beam (a few tens of meV for a wavelength of about 1 Å) is very low, a factor 1000 less than electrons for a similar wavelength. This means that fragile samples can be investigated without any damage. Helium atoms can be focussed in a number of ways, but Fresnel zoneplates have achieved the smallest beam focus so far (1µm), where atoms are focussed in a circular diffraction grating via their de Broglie wavelength. The first transmission mode images created using this technique were published early 2008 [1]. The resolution of those images was limited by chromatic aberration as well as thermal stability and mechanical vibration.

In order to further improve the technique we have developed a new fabrication process for free-standing Fresnel zoneplates to be used as focusing elements in a scaled-down and stabilised

setup designed to improve resolution to about 300 nm (full width half maximum) and create the first reflection mode images. Helium atoms at low energy generally do not penetrate material, which is why the circular grating structure is designed to be free-standing and only supported by radial support bars. The quality of the images obtained using this technique will strongly depend on the diffraction efficiency of the fabricated zoneplates, which is determined by how closely the zoneplate resembles the ideal grating pattern. Standard electron-beam lithography (We used the RAITH 150 system available at RLE's SEBL facility) provides the necessary resolution to create the outermost zones of 100 nm period and approximately 50% duty cycle, but pattern fidelity is limited by intra- and inter-writefield distortion. We have successfully developed a fabrication process for the free-standing zoneplates and we are currently working on minimizing both mentioned distortion errors using interference lithography gratings as a reference [2].

We have fabricated zoneplates (shown in figures 1 and 2) for different de Broglie wavelengths of the neutral helium beam and tailored to the new neutral helium microscope's experimental setup. These have a diameter of 196 μm and were thus created using a single 200μm writefield. Larger zoneplates created using multiple writefields have the potential of a higher intensity focus, which is clearly desirable for the microscopy tool. We have successfully extended the fabrication process to zoneplates created using four adjacent writefields (see figure 6), which causes inter-writefield distortion in the zoneplate pattern (see figure 5). Our current efforts are focussed on reducing this error using a segmented-fiducial-grid approach (see figure 3). The segmented fiducial grid (see figure 4) was created using Mach Zehnder interference lithography (Space Nanotechnology Laboratory), whose high degree of spatial coherence makes it an ideal 'ruler' on the nano-scale.

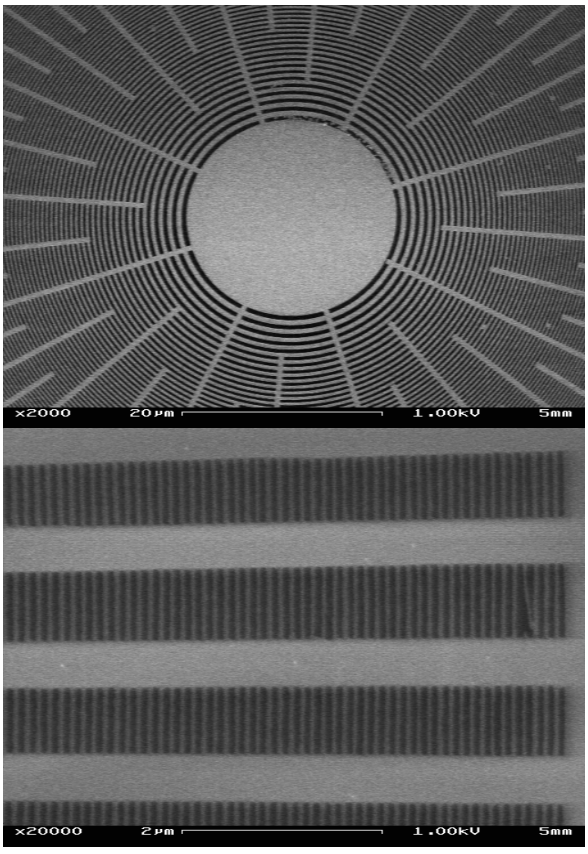

Figure 1: Scanning electron microscopy (SEM) micrographs of the free-standing silicon nitride zoneplates for a room temperature nozzle beam. The left image shows the centre of the zoneplate including the 20-μm-diameter stop and radially emanating support bars. The image on the right shows the 50-nm-wide outermost zones.

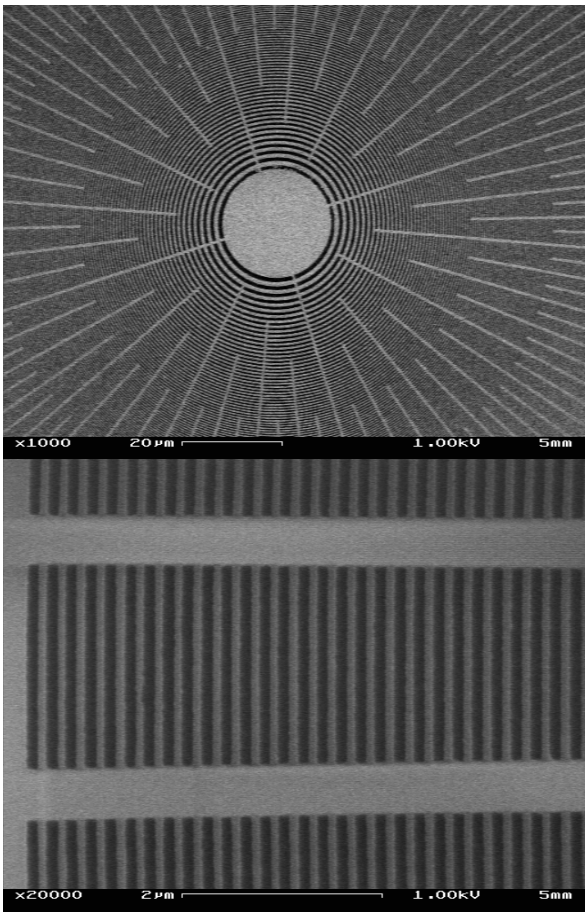

Figure 2: SEM micrographs of the free-standing silicon nitride zoneplates a cooled nozzle beam. The left image again shows the centre of the zoneplate while the image on the right depicts the 100-nm-wide outermost zones.

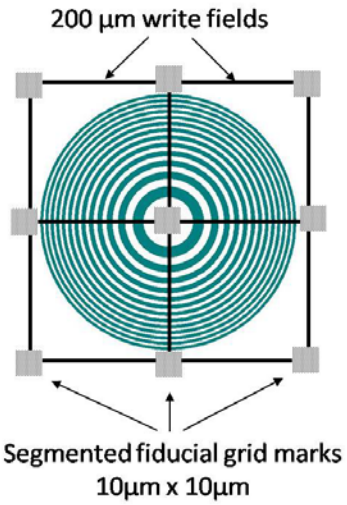

Figure 3: Schematic of spatial-phase locking approach for a zoneplate pattern using a segmented fiducial grid. The marks at the corner of the 200-µm writefields are dot-grids with a period of 200 nm, which were created by segmenting a Mach Zehnder interference lithography grid. They are used to align the writefield to the substrate as well as relative to each other, by scanning the write-field at the corners which are not relevant to the zoneplate pattern. The result will be a zoneplate with higher diffraction efficiencies.

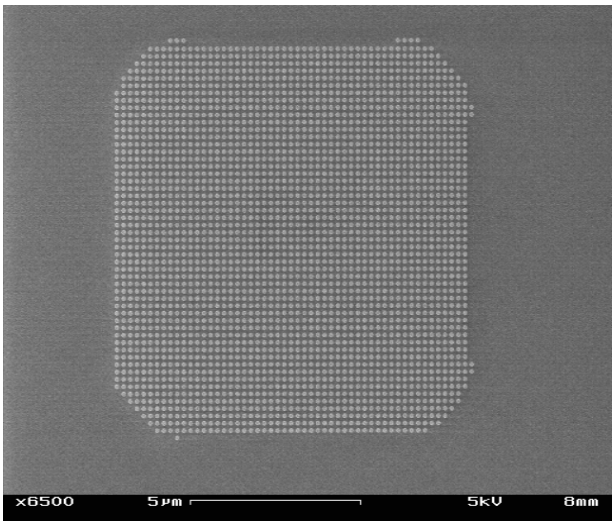

Figure 4: SEM micrograph of the approximately segmented-grid alignment-mark. The titanium-gold dots are arranged in a 200-nm grid, where the two grid-axes subtend an angle of 90° to an accuracy of better than 1 arc minute. The segmentation was achieved using standard contact-ultraviolet-lithography. The spatial phase of these marks is measured for each write field by two orthogonal line scans and the writefield alignment is updated based on that spatial phase at three writefield corners.

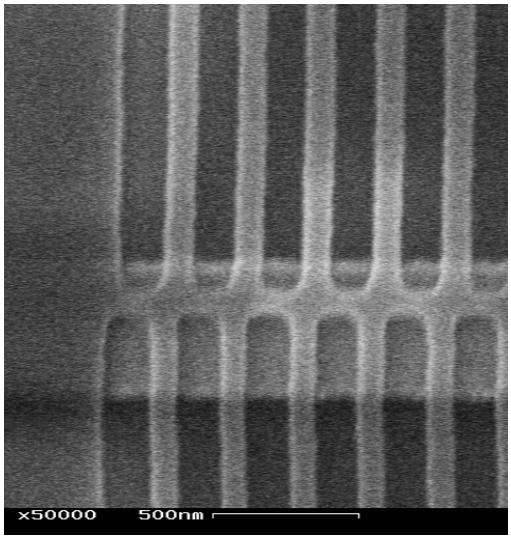

Figure 5: SEM micrograph of a zoneplate mask at a writefield border created without spatial-phase locking. The inter-writefield distortion is clearly visible as the 'stitching-error' located on top of the horizontal support bar and measures about 50 nm.

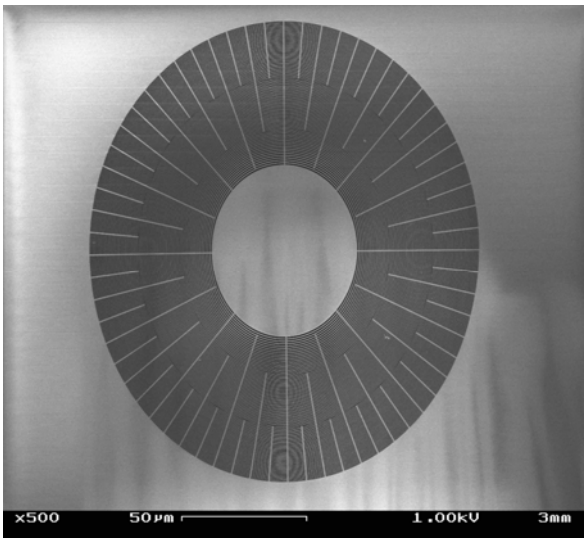

Figure 6: SEM micrograph of an entire 390-µm-diameter free-standing zoneplate created without spatial-phase-locking. Immediately visible are the radial support bars and the central disc blocking part of the zero diffraction order. Discontinuities in the Moiré patterns visible at the writefield borders hint at the pattern error we aim to reduce.

References:

[1] M. Koch, S. Rehbein, G. Schmahl, T. Reisinger, G. Bracco, W. E. Ernst, and B. Holst, J. Mic. (cover story) 229, 1 (2008). See also Nature Research Highlights: Nature 451, p.226-227, 2008.

[2] J. T. Hastings. Nanometer-Precision Electron-Beam Lithography with Applications *in Integrated Optics.* PhD thesis, Massachusetts Institute of Technology, June 2003.

Microscopy Beyond the Diffraction Limit Using Absorbance Modulation

Sponsors:
MIT Deshpande Center

Project Staff:
Dr. Rajesh Menon, Hsin-Yu Tsai, Prof. Henry I. Smith

Absorbance Modulation Imaging (AMI) is an approach to overcome the optical diffraction limit in the far–field, thereby achieving macro-molecular resolution with photons. Preliminary experiments show promising results that agree well with theoretical predictions [1].

AMI relies on an absorbance-modulation layer (AML), composed of photochromic molecules. Illumination at one wavelength, λ_2, renders the AML opaque, while illumination at a shorter wavelength, λ_1, renders it transparent. When illuminated with a ring-shaped spot at λ_2 co-incident with a focused spot at λ_1, the dynamic competition results in a nanoscale aperture, through which λ_1 can penetrate to the substrate beneath, as illustrated in Figure 1. The size of the aperture is limited only by the photo-kinetic parameters of the AML and the intensity ratio of the two illuminating wavelengths, not the absolute intensities [2]. By scanning this dynamic nanoscale aperture over the sample, resolution beyond the far-field diffraction limit is achieved. A related technique was demonstrated in stimulated-emission-depletion (STED) fluorescence microscopy [3]. However, while STED requires high power pulsed illumination and fluorescent markers, AMI can operate at low illumination intensity. A schematic of an AMI microscope is shown in Figure 2, in which collimated beams at λ_1 and λ_2 illuminate the *dichromat*, a binary phase element that creates a ring-shaped spot at λ_2 and a round spot at λ_1.

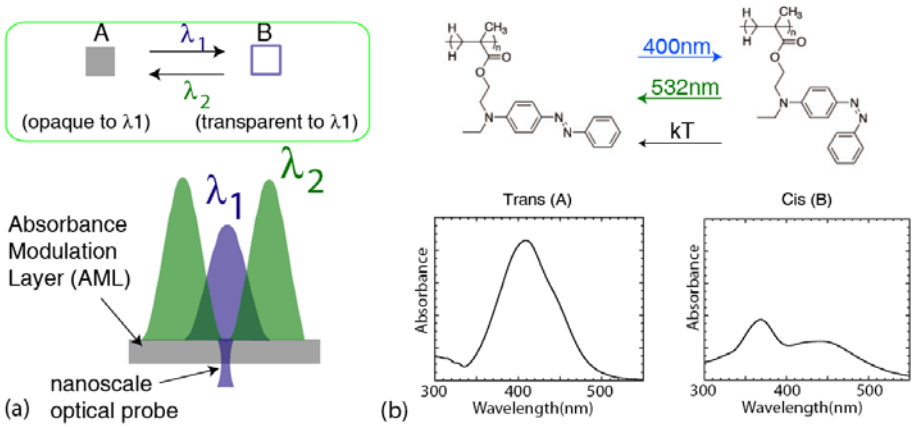

Figure 1: (a) Concept and illumination configuration for absorbance modulation. Through dynamic competition of the reversible transitions in the AML, the ring illumination at λ_2 creates a sub-wavelength aperture for λ_1. (b) The AML used in this Letter is composed of a polymer containing the photochromic azobenzene side chain, shown at the top. Upon exposure to 400 nm light, the trans isomer undergoes a photoisomerization reaction forming the cis isomer. The reverse reaction is favored upon exposure to 532 nm light or thermal excitation. The absorbance of the two isomers at λ_1=400 nm are markedly different.

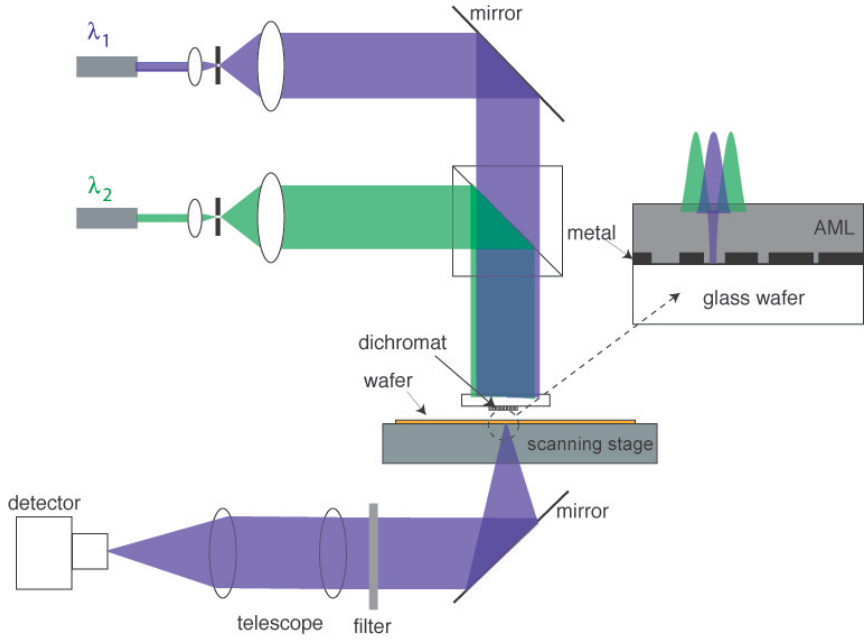

Figure 2: Schematic of absorbance-modulation imaging (AMI) microscope. The ring illumination at λ_2 creates a local subwavelength aperture for λ_1 in the AML through which the underlying object is illuminated and the scattered light collected. Multiple dichromats generate separate signals, enabling parallelism and enhanced throughput. The inset shows a schematic of a resolution test structure consisting of metal lines on a glass wafer.

Dichromats composed of concentric circular zones whose radii and phase shift are selected based on a nonlinear-optimization algorithm [4].The dichromats can readily be fabricated using electron beam lithography in dielectric materials, such as poly-methylmethacrylate (PMMA) or hydrogen silsesquioxane (HSQ), enabling the fabrication of large arrays of dichromats with high optical uniformity [5]. Figure 3 shows the fabrication process and scanning-electron micrographs of the dichromats. The point-spread functions of these dichromats were verified through photoresist exposures and PSF compression via absorbance modulation was demonstrated in lithography with NA=0.55 dichromats. As indicated in Figure 4, λ_1 illumination is focused more tightly as the intensity at λ_2 is increased relative to that at λ_1. The full-width at half-maximum (FWHM) of the λ_1 PSF decreased from 300 nm to 250 nm when the ratio of the intensity at λ_2 to that at λ_1 is 20, illustrating the tighter focusing enabled by absorbance modulation.

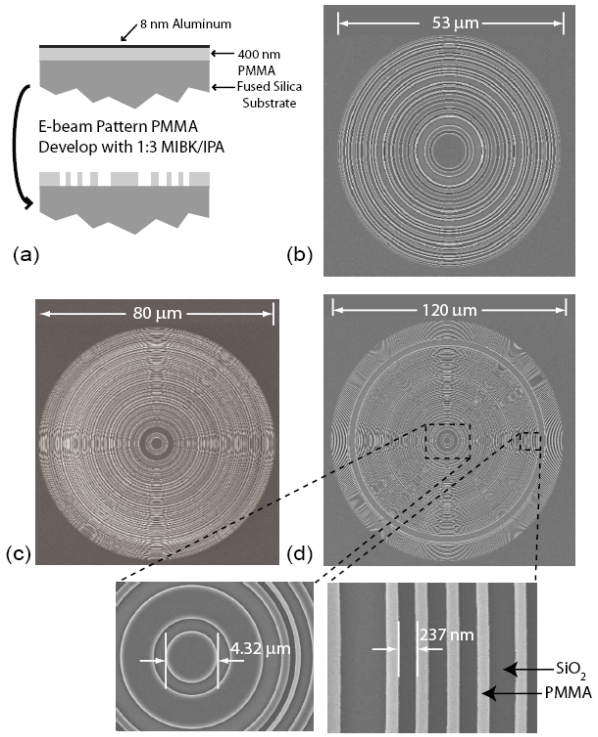

Figure 3: (a) Schematic of the fabrication process of the dichromats. PMMA was spun on top of a fused silica substrate, and a thin layer of aluminum was evaporated on top as a conduction layer. Exposed PMMA was developed in a solution of MIBK and IPA in the ratio of 1:3. Scanning-electron micrographs of the fabricated dichromats with (b) NA=0.55, (c) NA=0.7, and (d) NA=0.83. The moiré artifacts are a consequence of image formation via scanning. Insets at the bottom show magnified images of the NA=0.83 dichromat. Note that the sequence of zone radii differs significantly from that of a Fresnel zone plate.

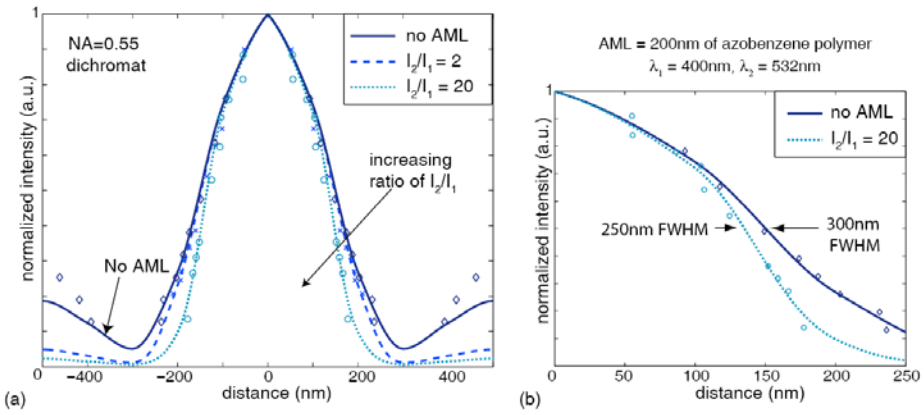

Figure 4: Experimental demonstration of PSF compression via absorbance modulation in lithography using a dichromat with 0.55 NA. λ_1 and λ_2 are the incident intensities at λ_1 and λ_2, respectively. (a) The solid line shows the simulated PSF at λ_1 when no AML is present. The diamonds show the corresponding experimental data. The dashed line shows the simulated PSF at λ_1 when I_2/I_1=2. The crosses show the corresponding experimental data. The dotted line shows the simulated PSF at λ_1 when I_2/I_1=20. The circles represent the corresponding experimental data. As I_2/I_1 increases, the λ_1 illumination beyond the film is focused more tightly. (b) Expansion from (a) indicating FWHM compression from 300nm to 250nm. Least-squares fits were conducted separately on each set of data to obtain the I_2/I_1=2 and I_2/I_1=20 ratios.

References:

[1] R. Menon, H-Y Tsai, and S. W. Thomas III, "Far-field generation of localized light fields using absorbance modulation," *Phys. Rev. Lett.* 98(4): 043905 (2007).

[2] R. Menon and H. I. Smith, "Absorbance modulation optical lithography," *J. Opt. Soc. Am. A* 23(9): 2290-2294 (2006).

[3] S.W. Hell and J. Wichmann, "Breaking the diffraction resolution limit by stimulated emission: stimulated-emission-depletion fluorescence microscopy," *Optics Lett.* 19(11): 780-782 (1994).

[4] Rajesh Menon, Paul Rogge, and Hsin-Yu Tsai, "Design of diffractive lenses that generate optical nulls without phase singularities," J. Opt. Soc. Am. A, 26(2), 297 (2009).

[5] Dario Gil, Rajesh Menon, and Henry I. Smith, "Fabrication of high-numerical-aperture phase zone plates with a single lithography exposure and no etching," J. Vac. Sci. Technol. B 21, 2956-2960 (2003).

Publications

Journal Articles, Published

1. Hsin-Yu Tsai, Henry I. Smith, and Rajesh Menon, "Reduction of focal-spot size using dichromats in absorbance modulation," Optics Letters, 33(24), 2916 (2008).
2. Rajesh Menon, Paul Rogge, and Hsin-Yu Tsai, "Design of diffractive lenses that generate optical nulls without phase singularities," J. Opt. Soc. Am. A, 26(2), 297 (2009).

Conference Presentations

1. Rajesh Menon, Hsin-Yu Tsai, and Trisha L. Andrews, "Generating Optical Near-Fields from Afar via Absorbance Modulation," Frontiers in Optics/ Laser Science XXIV Conference, Oct., 2008.

Localized Substrate-Removal Technique Enabling Strong-Confinement Microphotonics in Bulk-Silicon CMOS

Sponsors
DARPA

Project Staff
Dr. Charles. W. Holzwarth, Jason S. Orcutt, Jie Sun, Hanqing Li, Milos A. Popovic, Prof. Vladimir Stojanovic, Prof. Judy L. Hoyt, Prof. Rajeev J. Ram, and Prof. Henry I. Smith

Efforts elsewhere to integrate photonics with CMOS electronics require customization of the fabrication process to provide low-loss photonic components [1]. This compromises electronic performance, throughput, and cost. Customizations included thick low-index cladding layers, silicon-on-insulator material and electron-beam lithography. While tolerable for some applications, such customization is considered unacceptable for microprocessors and DRAM, circuits that would benefit the most from optical intrachip communication. To integrate photonics with circuits produced in high volume, one must be able to work within the constraints of commercial bulk CMOS process flows by utilizing industry-standard material layers, thicknesses, processing steps and tools. The CMOS process flow allows waveguides to be fabricated out of the polysilicon layer used for transistor gates and poly-resistors deposited above the shallow-trench isolation (STI) layer. However, such waveguides have a propagation loss on the order of ~1000 dB/cm since

the STI layer (<400 nm) is not thick enough to prevent the guided optical mode from "leaking" into the high-index Si substrate.

To overcome this problem, we have developed a novel post-processing technique using XeF_2 to locally remove the silicon underneath the STI layer, as shown in Fig. 1. The creation of air tunnels under the polysilicon waveguides eliminates propagation loss due to leakage into the substrate, with minimal impact on the electrical, thermal, and mechanical performance of the electronics. XeF_2 gas is used because it etches Si isotropically, can undercut large areas without stiction problems, and has a high silicon-to-oxide etch-rate selectivity (>1000:1).

We have used this method to fabricate waveguides in polysilicon-on-oxide films, where the oxide undercladding was only 50 nm (Fig. 2). The propagation loss of these waveguides was measured to be ~10 dB/cm at 1550 nm. Most of this loss is attributed to material absorption and scattering from surface and sidewall roughness [2]. We have also shown that this process can be performed as a postprocessing step on commercial CMOS chips. Using CF_4 based reactive-ion etching it is possible to open vias through the dielectric stack exposing the Si substrate. Once exposed XeF_2 can then be used to locally remove the substrate, undercutting the proximate photonic structures (Fig. 3).

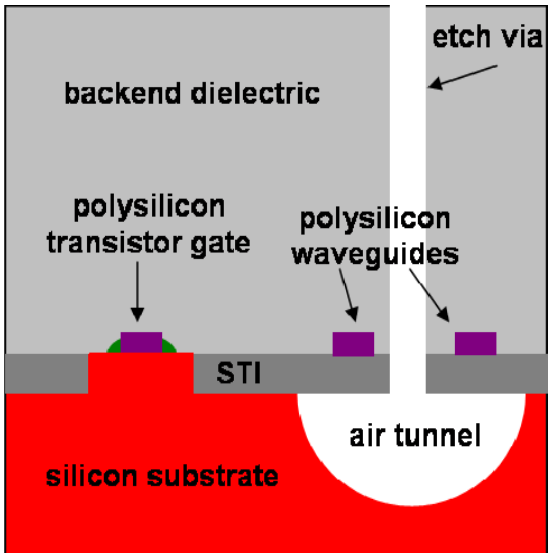

Figure 1: Sketch of the cross-section of a bulk CMOS chip showing how electronics and photonic devices can be fabricated on the same chip with only the addition of a post-processing step to locally remove the silicon substrate beneath the polysilicon waveguides.

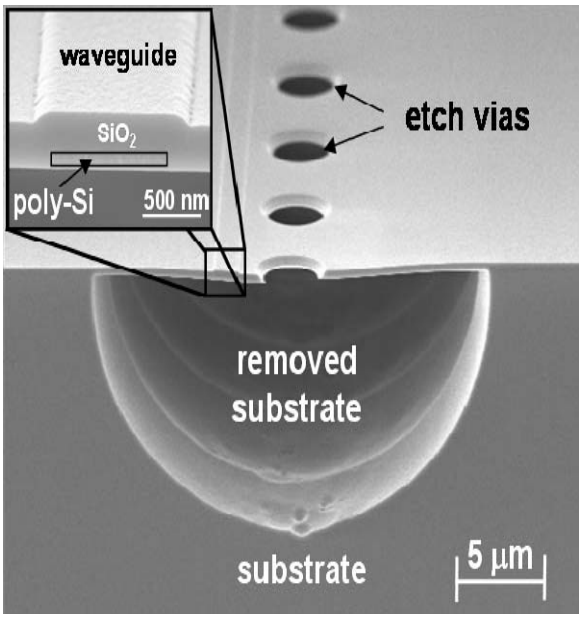

Figure 2: Scanning-electron micrograph of fabricated poly-silicon waveguide using the XeF_2 based substrate removal technique. The inset shows a close-up of the waveguide. The SiO_2 cladding beneath the poly-silicon is only 50 nm thick resulting in loss >1000 dB/cm before the localized substrate removal step. After removal, the loss is reduced to approximately 10 dB/cm.

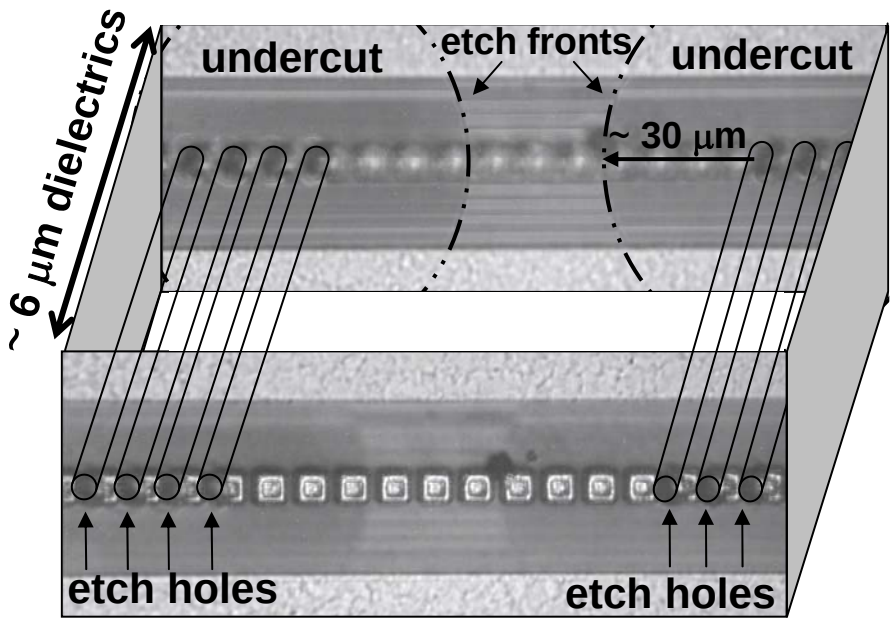

Figure 3: Optical micrographs showing the localized substrate removal processes performed to release waveguides on a 65 nm node CMOS chip. The lower picture is focused on the top surface and the upper image is focused on the waveguide layer located below ~ 6 mm of dielectrics. The XeF_2 etch fronts are labeled.

References:

[1] J.S. Orcutt *et al*., "Demonstration of the first electronic photonic integrated circuit in a commercial scale bulk CMOS Process," Submitted to the Conference of Lasers and Electro-Optics (CLEO), San Jose, California, May 5-9, 2008.

[2] C.W. Holzwarth *et al*., "Localized Substrate Removal Technique Enabling Strong-Confinement Microphotonics in Bulk-Si CMOS Processes," Submitted to the Conference of Lasers and Electro-Optics (CLEO), San Jose, California, May 5-9, 2008.

Nanofabrication of Optical Microring Filter Banks for Integrated Photonic Systems

Sponsors:
DARPA

Project Staff:
Dr. Charles W. Holzwarth, Tymon Barwicz, Milos A. Popović, Anatoly Khilo, Marcus Dahlem, Prof. Erich P. Ippen, Prof. Franz X. Kärtner and Prof. Henry I. Smith

Progress in designs and nanofabrication techniques for microring-resonators in high-index-contrast materials have made possible the wide spectral spacing between resonances and low loss required for electronic-photonic integrated circuits, including ultra-fast analog-to-digital converters [1]. Achieving accurate resonant-frequency spacing of microring-filters is critical for these devices. In the NanoStructures Laboratory we have developed a technique using scanning-electron-beam lithography (SEBL) that is capable of accurately controlling the resonant frequency spacing in microring-resonator filter banks. The resonant wavelength of a microring-

resonator filter is dependant on the ring radius and the effective index of refraction of the ring waveguide. The effective index is controlled lithographically by controlling the width of the ring waveguide. Although it is simple to change the width and the radius of the ring in the SEBL layout, this is limited to discrete jumps corresponding to the step size of the SEBL address grid. In order to have 1 GHz control of the resonant frequency for the designed filters the SEBL systems would need a step size of 30 pm. In our process this limitation of discrete step size is overcome by modulating the electron beam dose to precisely control the average width of the ring waveguide [2]. However, stochastic variations during processing typically limit dimensional precision to ~0.5 nm (frequency errors of a ~10 GHz), resulting in the need for postfabrication trimming. Ideally, one would have the means to dynamically and statically trim the resonant frequency of each microring. For dynamic trimming, we have integrated microheaters, taking advantage of the temperature dependence of the refractive index. For static trimming, we are developing an electron-beam curing process that changes the refractive index of the hydrogen silsesquioxane (HSQ) overcladding. These two methods enable the efficient correction of resonant frequency errors in filter banks.

In our experiment second-order microring-resonator filters, fabricated in silicon-rich silicon nitride and overclad with HSQ, were used in a microring filter banks (Fig. 1(a), (b)). Using dose modulation, twenty-channel dual-filter banks with a target channel spacing of 80 GHz were fabricated and tested, demonstrating control of changes in the average ring-waveguide width of 0.10 nm, despite the 6 nm SEBL step size (Fig. 1(c)). Variations between filter responses were due to slight frequency mismatches between rings of the same filter, we demonstrated that this can be corrected by thermal trimming with integrated microheaters (Fig. 2).

Our current efforts are focused on improving filter bank performance, by using lower loss Si-core microring resonators and developing a static-trimming technique. The transmission response of a two-channel Si filter bank demonstrates the low drop loss (1.5 dB) and crosstalk (-33 dB) achievable with Si filters (Fig. 3). Also, initial experiments have shown that we can statically shift the resonant frequency of a microring by electron-beam curing the HSQ overcladding (Fig. 4).

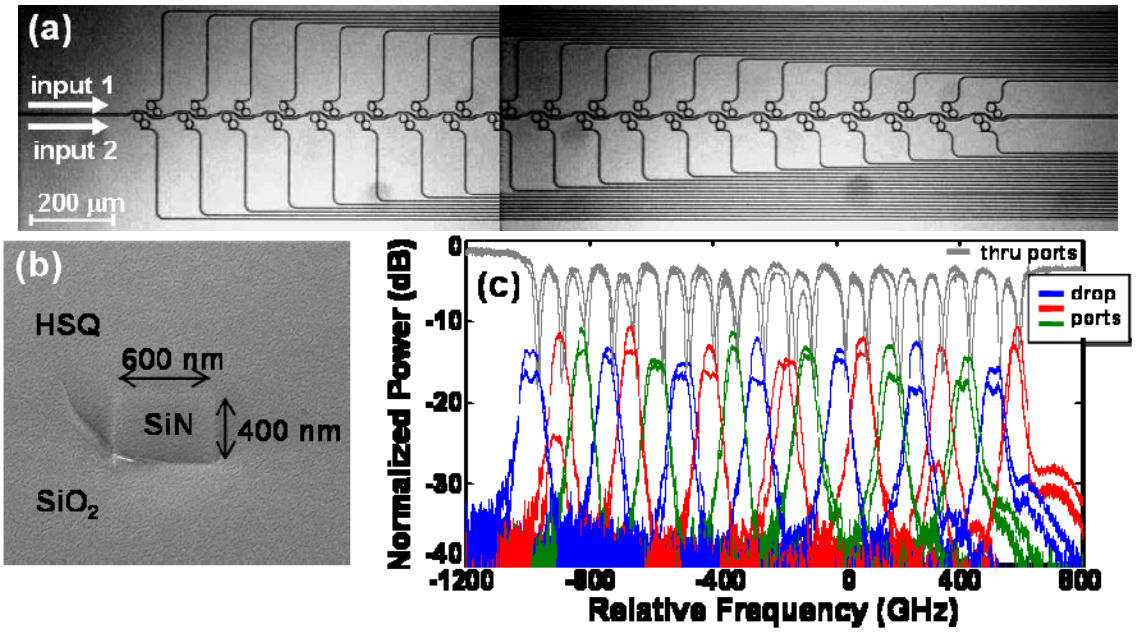

Figure 1: a) Scanning-electron micrograph of fabricated second-order twenty-channel dual-filter bank and b) cross-section of overclad waveguide. c) Filter response of second-order twenty-channel dual-filter bank with an average channel spacing of 83 GHz.

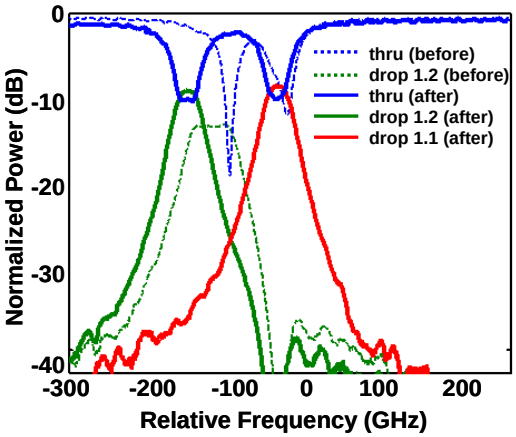

Figure 2: Transmission response of the two-channel SiN_x filter bank before and after using thermal trimming to correct frequency errors.

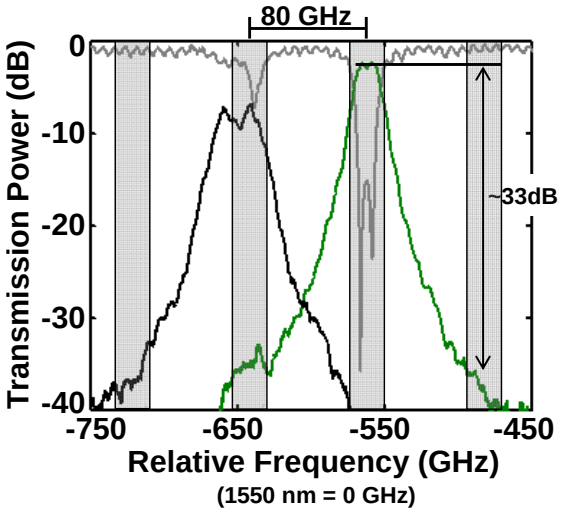

Figure 3: Transmission response of two-channel Si filter bank. The two rings that comprise the filter for the right drop response (green) have a frequency mismatch of 0.4 GHz resulting in a drop loss of only 1.5 dB.

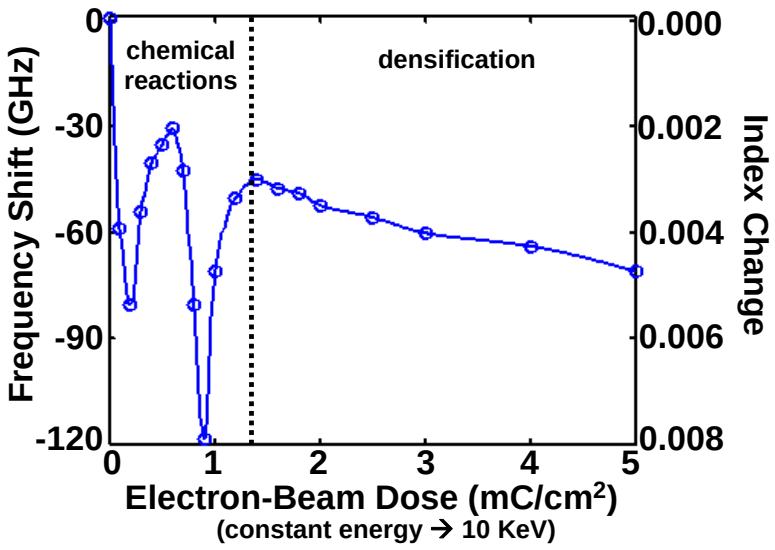

Figure 4: Static frequency shift versus electron-beam dose for a Si-microring filter with 110 nm of HSQ overcladding. At lower dose the frequency shifts are caused by chemical reactions and at higher dose the frequency shifts can be explained by densification of the HSQ structure. The right axis shows the corresponding change in refractive index of the HSQ for the frequency shift.

References:

[1] T. Barwicz, M.A. Popovic, P.T. Rakich, M.R. Watts, H.A. Haus, E.P. Ippen, H.I. Smith, "Microring-resonator-based add-drop filters in SiN: fabrication and analysis," *Optics Express* 12(7): (2004).

[2] C.W. Holzwarth, T. Barwicz, M. A. Popović, P. T. Rakich, F. X. Kaertner, E. P. Ippen, and H. I. Smith, "Resonance-frequency control of high-index-contrast microphotonic cavities at fabrication," *JVST B* 24(6): (2006).

Correction of Intrafield Distortion in Scanning-Electron-Beam Lithography and Confirmation via Optical Ring-Resonator Filters

Sponsors:
DARPA

Project Staff:
Jie Sun, Charles W. Holzwarth, Prof. Jeffrey T. Hastings (U. Kentucky), Prof. Henry I. Smith

In scanning-electron-beam lithography (SEBL), distortion in the electron-beam deflection field (i.e., intrafield distortion) leads to systematic pattern-placement errors. These are particularly detrimental to photonic devices, which depend on coherent interference. Intrafield-distortion arises from imperfections in the electron optics, and errors in the digital-to-analog conversion and field-calibration electronics. The intrafield-distortion of our Raith 150 SEBL system was measured by comparing a written grid to a precision reference grid, generated by interference lithography. Figure 1(a) and 1(b) illustrate maps of the Raith's intrafield-distortion for a 100mm field in x and y direction, respectively.

Optical microring-resonator filters in high-index-contrast materials, such as Si or Si_3N_4, require 1-nm-level pattern placement precision. In fabricating such devices with SEBL, intrafield-distortion is manifested in the deviation of resonant frequency from design values. Based on the measured distortion maps, we calculated the expected resonant-frequency mismatch as a function of filter position and orientation in the SEBL exposure field. Figure 2 shows the results, with the dots representing experimental results and continuous lines representing simulation results. The near agreement between our model and experiments confirms the earlier measurement of intrafield-distortion. Based on the distortion maps, we corrected the intrafield-distortion in second-order microring-resonator filters by pre-distorting the beam positions in the layout. Figure 3(a) and 3(b) show the statistical results of resonant-frequency mismatch without and with intrafield-distortion correction, respectively. By applying distortion correction, the average resonant-frequency mismatch is reduced from -8.6GHz to 0.28GHz.

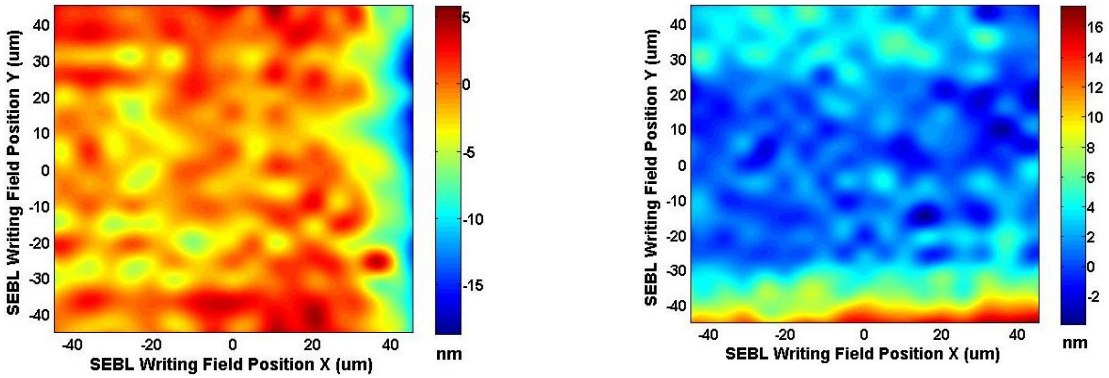

Figure 1: Intrafield-distortion in (a) x and (b) y direction in a Raith 150 SEBL system. The two-dimensional quasi-periodic character of the distortion (i.e. the quasi-periodic peaks and valleys in the above distortion maps) is probably indicator of imperfection in the digital-analog converter.

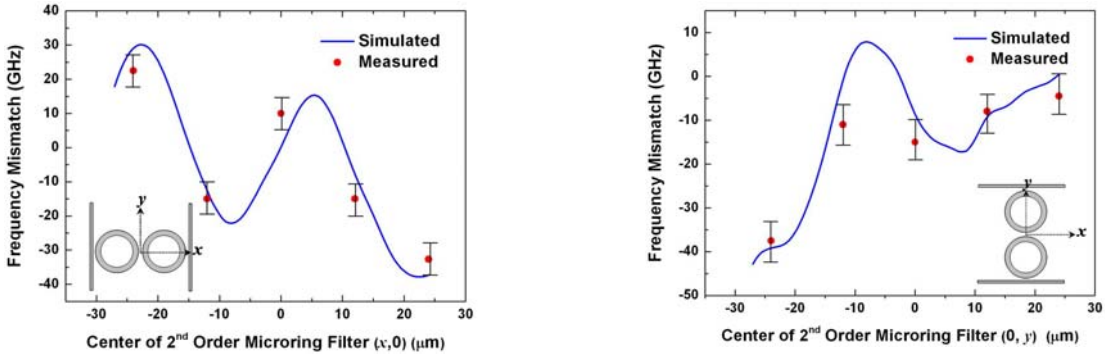

Figure 2: Frequency mismatch between the two rings of second-order microring filters at various positions in the SEBL writing field: (a) the positions of the center of the second-order filter are at y =0 and various values of x, from x= -24 μm to x = +24 μm, and (b) the positions of the center of the second-order filter are at x =0 and various values of y from y = -24 μm to y = +24 μm. The inset diagrams illustrate the orientations of the filters in the two cases.

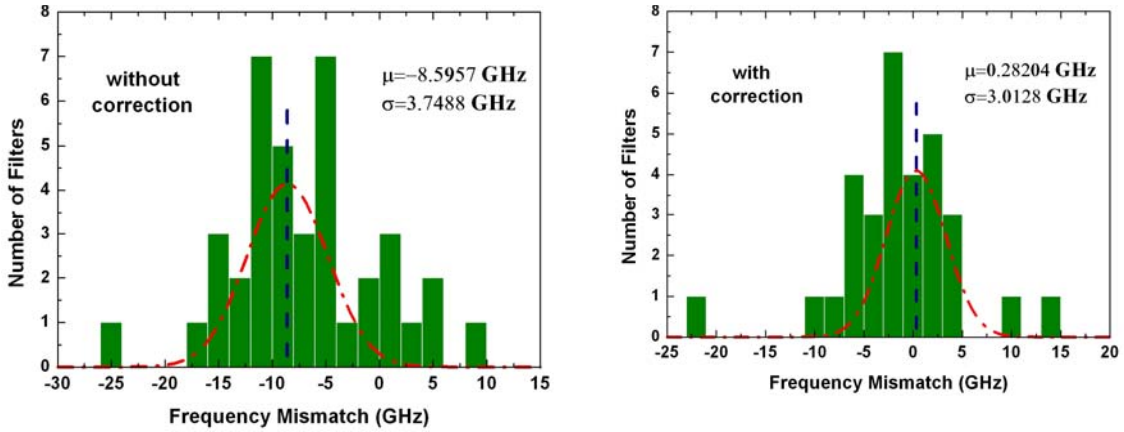

Figure 3: Statistics of frequency mismatch of a number of second-order filters at several positions in the SEBL writing field, where μ is the average frequency mismatch, and σ is the standard deviation of frequency mismatch: (a) without distortion correction and (b) with distortion correction. Note that the correction results in a reduction of μ from -8.6GHz to 0.28GHz.

References:

[1] Jie Sun, Charles W. Holzwarth, Marcus Dahlem, Jeffrey T. Hastings, and Henry I. Smith, "Accurate frequency alignment in fabrication of high-order microring-resonator filters," Optics Express, vol. 16, no. 20, 15958-15963 (2008)

Design and Fabrication of Sampled Bragg Gratings in SOI

Sponsors:
DARPA

Project Staff:
Jie Sun, Charles W. Holzwarth, Prof. Henry I. Smith

Waveguide Bragg gratings are used in optical communication systems for many applications. However, in order to achieve more advanced grating properties, such as phase shift and chirp, Scanning-Electron-Beam-Lithography (SEBL) with special precision-control techniques (e.g. Spatial-Phase-Locked EBL) represents one approach. We propose a novel sampled-Bragg grating (SBG) structure to realize various grating responses using optical lithography only. In this scheme, interference lithography is used to fabricate the background grating with excellent coherence, and then the background grating is amplitude-modulated to achieve various grating responses.

A schematic diagram of the SBG is shown in Fig. 1. In SBG, various grating responses are realized by reallocating the sampling positions and by varying the duty cycle of each sampling. For example, the phase shift grating is achieved by phase shifting the sampling instead of the grating itself. Figure 2(a) shows the simulated transmission spectrum of a phase shift grating using SBG, where the desired filter response appears in the -1st channel. Similarly, the chirp grating is achieved by chirping the sampling period, as shown in Fig. 2(b).

The sampling period is usually of the order of ~10μm, which is much larger than the grating period and enables to use optical-contact lithography only to fabricate such SBG. A processing flow for SBG fabrication was developed. A thin layer of SiO_2 was first evaporated on top of an SOI wafer. The background grating was formed on this layer through interference lithography.

This SiO_2 grating layer will serve as a hard mask to etch grating into silicon later. Then the sampling pattern was transferred onto the grating layer by optical-contact lithography and etching away excess background grating. After this, a second contact lithography was performed to pattern the waveguides and HBr etching was used to transfer the waveguide pattern into silicon to form a ridge waveguide. Finally, the grating pattern was etched into the top of the silicon ridge waveguide to a certain depth to form the SBG. Figure 3(a) shows the micrograph of a fabricated SBG, and Fig. 3(b) shows the cross-sectional view of the SBG under Scanning-Electron-Microscope.

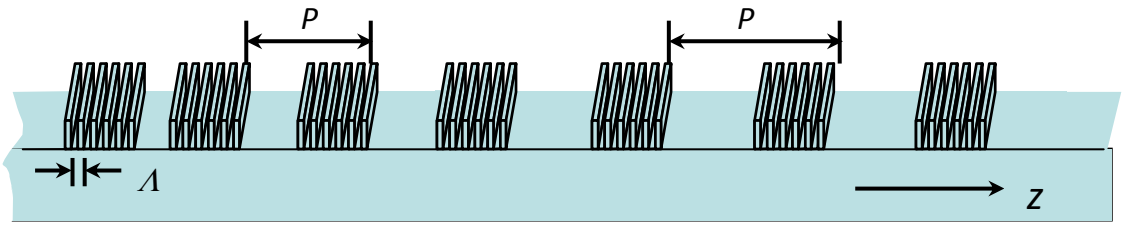

Figure 1: A schematic diagram of the Sampled Bragg grating

Quantum Nanostructures and Nanofabrication

RLE Groups
Quantum Nanostructures and Nanofabrication Group, NanoStructures Laboratory

Academic and Research Staff
Professor Karl K. Berggren

Postdoctoral Students
Stephan A. Schulz, Francesco Marsili, Sebastian Strobel

Graduate Students
Joshua Leu, Xiaolong Hu, Jae-Byum Chang, Donald Winston, Vitor Manfrinato, David Meyer

Visiting Students
Huigao Duan, Charles Herder, Adam McCaughan, Faraz Najafi, Hasan Korre, Lorenzo Battistella

Technical and Support Staff
James Daley, Mark Mondol, Alicia Akins, Denise Stewart

The Quantum Nanostructures and Nanofabrication Group investigates the application and fabrication of devices using the foundations of quantum mechanics. We focus on: superconductive devices and materials applied single-photon detection and quantum computing; nanofabrication methods; and applications of nanofabrication to energy systems. Superconductive devices are among the most readily engineered examples of devices exhibiting quantum-mechanical effects. We therefore work with superconductive materials, including efforts in materials, processing, and analysis. Also, because quantum-mechanical effects are primarily observable at microscopic length scale, we develop and implement novel methods of nanofabrication. We take a multi-disciplinary approach to these topics, borrowing techniques from physics, electrical-engineering, computer science, chemistry, and materials science.

Transmission-Electron-Microscopy-based Metrology of Sub-10-nm Electron-beam Lithography

Sponsors:
NRI, INSIC, Alfaisal University and King Abdulaziz City for Science & Technology

Project Staff:
H. Duan, J. Yang, B. Cord, K. K. Berggren
Research Laboratory of Electronics, MIT

Ultrahigh resolution electron-beam lithography has promising applications to bit-patterned media, high-resolution and templated self-assembly, sub-10-nm nanoelectronic devices, and mask manufacturing for integrated circuits. Much progress has been made on ultrahigh resolution electron-beam lithography (EBL) in recent years with the help of new tools, new resists, and new resist development processes. Sub-5-nm half-pitch features have been fabricated using salty development [1] on HSQ resist using Raith 150^{TWO} [2]. It is believed that the resolution can be further improved with the efforts of using smaller electron-beam spot size and continuous optimizing the resist development process. However, when EBL is approaching its limit, metrology poses an increasing difficulty.

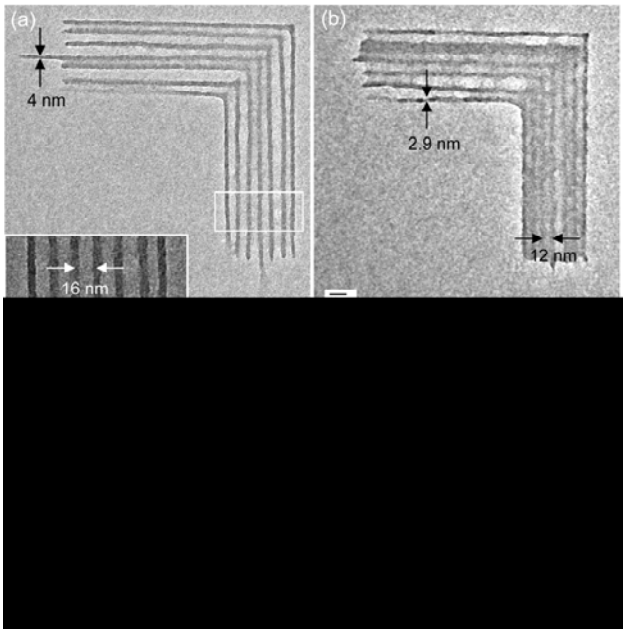

Figure 5: TEM images of (a) 16-nm-pitch and (b) 12-nm-pitch structures fabricated using the Raith 150 at MIT with 32-nm-thick HSQ resist on silicon nitride membranes. The accelerating voltage was 30kV, and the working distance was about 6 mm. The TEM images were taken by using a JEOL JEM 2010 with an accelerating voltage of 200 keV.

First, it is well-known that size distribution, line-edge roughness, line width roughness, and position placement accuracy caused by random events (such as system instability, shot noise, random interaction of electrons and resists, and random interaction of resists and developers) are very important parameters for practical applications. These random events become more obvious and much more important when the resolution approaches the nanometer scale, so it is essential to understand them. However, considering a variance of 10% of a 5-nm half-pitch, the size deviation should be less than 0.5 nm, which poses a challenge to even the best scanning-electron microscope. Second, ultrahigh resolution electron-beam lithography is intrinsically different from traditional electron-beam lithography. For example, ultrathin resists must be used,

the electron distribution of the electron beam plays a more important role at the resolution, secondary electrons may also have a big effect on the lithography, the development process becomes less controllable, and even minor defects become fatal to devices. To study and to control such effects, morphological details must be ascertained prior to subsequent processes. Third, for many nanoelectronic applications, critical dimension must be controlled on the order of 0.1 nm.

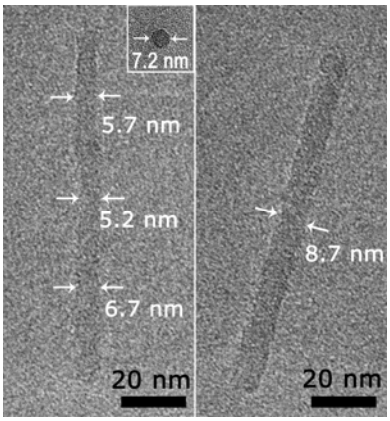

Figure 6: TEM images of fallen-over single dots with a diameter of about 6 nm (a) and 8 nm (b) using 120-nm-thick HSQ as resist. All other parameters were the same as those in Figure 1. This image indicates that 30kV electron beam could pass through 120-nm-thick HSQ with a very small scattering angle, and the aspect ratio of the dot approached 20. Inset is the top view of thinner post at the same dose.

Considering the above-mentioned points, we have adopted High-Resolution Transmission-Electron Microscopy (HRTEM) to approach a metrology accuracy order of 0.1 nm and investigate the morphological and structural details of ultrahigh resolution electron-beam lithography. Figure 1 shows the comparison of typical TEM images and SEM images [3], from which more details can be found and the dimension of the structures can be precisely measured. Figure 2 shows sub-10-nm fallen-over dots [3], from which much information about forward scattering can be obtained.

References:

[1] J. K. W. Yang and K. K. Berggren, “Using high-contrast salty development of hydrogen silsesquioxane for sub-10-nm half-pitch lithography,” *J. Vac. Sci. Technol. B*, vol. 25, pp. 2025-2029, (2007).

[2] J. K. W. Yang, B. Cord, and K. K. Berggren, “Understanding of Hydrogen Silsesquioxane Electron Resist for Sub-5nm-Half-Pitch Lithography,” to be published.

[3] H. G. Duan, J. Yang, B. Cord, K. K. Berggren, “Transmission-electron-microscopy-based Metrology of sub-10-nm electron beam lithography,” in preparation.

Lithography with a scanning beam of helium ions

Sponsors:
NRI, NSF GRFP

Project Staff:
D. Winston, B. M. Cord, M. K. Mondol, J. K. W. Yang, K. K. Berggren
Research Laboratory of Electronics, MIT

B. Ming, A. E. Vladar, M. T. Postek
National Institute of Standards and Technology

D. C. Bell
Harvard University

W. F. DiNatale, L. A. Stern
Carl Zeiss SMT

Scanning-electron-beam lithography (SEBL) is a versatile technique to rapidly prototype devices with a spatial resolution of tens of nm. Recent work in our group has pushed the resolution of SEBL to less than 10 nm by careful selection of materials and processes [1]. However, SEBL is intrinsically limited in resolution by the nature of electrons. No matter how tightly a beam of electrons is focused onto the surface of a resist, the focused energy will spread through the resist in the form of scattered primary electrons and generated secondary electrons. Electrons are light in mass, and thus scatter easily in a resist and generate secondary electrons with a long range. Because heavier particles should scatter less and should transfer less of their kinetic energy to secondary electrons, prior work has considered particles such as H_2^+, He^+, and Ga^+ for scanning-beam lithography [2-4]. Unfortunately, systems built for evaluating lithography with ions have until now been limited by either source brightness and thus by achievable focus, or by damage resulting from the ion being too heavy relative to constituents of a typical resist.

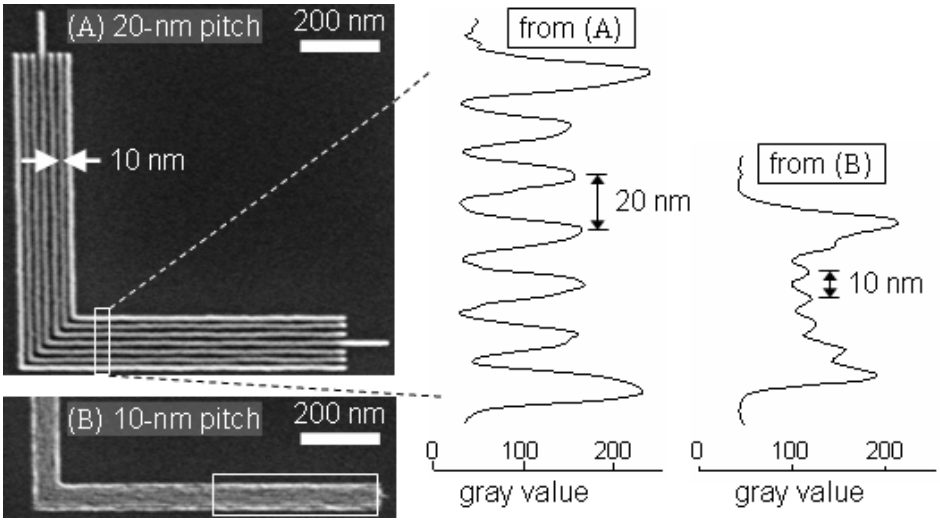

Figure 7: (A) Scanning electron micrograph of 10-nm-half-pitch nested-Ls of 25-nm-thick HSQ on silicon; line dose was 0.232 nC/cm (exposure step size was 1.25 nm, and dwell time per exposure point was 104μs). (B) A region of 5-nm-half-pitch nested Ls at the same imaging magnification as (A); the line dose was 0.083 nC/cm, or ~50 ions/nm (exposure step size was 1.25 nm, and dwell time per exposure point was 37.3μs). Averaging across each row of pixel values in the white-boxed areas obtains cross-sectional slices that show the modulation apparent in each nested-L structure.

The recent commercial availability of a scanning-helium-ion-beam microscope with high source brightness [5] has prompted us to evaluate the use of this microscope for lithography, with the hope of being able to prototype devices with a spatial resolution less than what we currently can achieve with SEBL. We connected a Zeiss Orion microscope to a Nabity NPGS pattern generator and successfully fabricated test structures in hydrogen silsesquioxane (HSQ) resist on silicon. As shown in Figure 3, we have fabricated 10-nm-half-pitch structures with little residue between features, and 5-nm-half-pitch structures with some fidelity. Also, we have used a sequence of point exposures [6] to estimate the point-spread function of scanning-helium-ion-beam lithography (SHIBL); our results suggest that the point-spread function of SHIBL may indeed be narrower than that of EBL [7], but additional validation is necessary. Furthermore, different resist materials and processes may be necessary to unleash the potential of SHIBL for lithography of higher resolution than EBL.

References:

[1] J. K. W. Yang and K. K. Berggren, "Using high-contrast salty development of hydrogen silsesquioxane for sub-10-nm half-pitch lithography," *Journal of Vacuum Science & Technology B (Microelectronics and Nanometer Structures)*, vol. 25, pp. 2025-9, 11 (2007).

[2] K. Horiuchi, T. Itakura and H. Ishikawa, "Fine pattern lithography using a helium field ion source," in *31st International Symposium on Electron, Ion, and Photon Beams*, pp. 241-4 (1988).

[3] R. L. Kubena, J. W. Ward, F. P. Stratton, R. J. Joyce and G. M. Atkinson, "A low magnification focused ion beam system with 8 nm spot size," in *35th International Symposium on Electron, Ion and Photon Beams,* pp. 3079-83 (1991).

[4] J. A. Van Kan, A. A. Bettiol and F. Watt, "Proton beam writing of three-dimensional nanostructures in hydrogen silsesquioxane", *Nano Letters*, vol. 6, pp. 579-582 (2006).

[5] S. A. Rishton and D. P. Kern, "Point exposure distribution measurements for proximity correction in electron beam lithography on a sub-100 nm scale," in *30th International Symposium on Electron, Ion, and Photon Beams*, pp. 135-41 (1987).

[6] B. W. Ward, J. A. Notte and N. P. Economou, "Helium ion microscope: a new tool for nanoscale microscopy and metrology," *Journal of Vacuum Science & Technology B (Microelectronics and Nanometer Structures),* vol. 24, pp. 2871-4, 11 (2006).

Sub-40-nm patterning of Au of GaAs for Nanowire Catalysis

Sponsors:
IBM, MARCO, MSD, NRI

Project Staff:
J. Leu, M. Brewster, S. Gradecak, K.K. Berggren
Research Laboratory of Electronics, MIT

In this work, we demonstrate sub-40-nm patterning of Au features on GaAs substrates using a bilayer-resist structure. Patterning of small Au features onto GaAs substrates is of particular interest due to their use as metal catalysts for GaAs and GaAs-alloy nanowire growth. Semiconducting nanowires have a variety of potential applications, such as field-effect transistors (FETs) [1], and their size-dependent properties have been exploited for a variety of optoelectronic devices [2]. However, due to the poor adhesion of metal catalysts to III-V materials, the use of metal-nanoparticle-catalysis in sub-50-nm diameter nanowire growth has been limited.

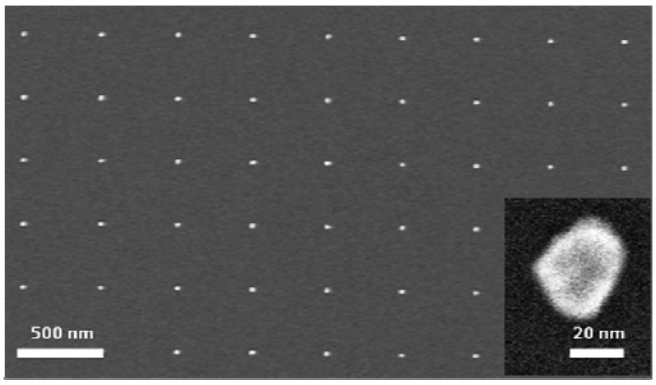

Figure 8: An array of sub-40-nm-diameter features consisting of a metal stack of 10-nm Au atop 3-nm Cr on a GaAs substrate, deposited by metal-evaporation onto a patterned PMMA/PMGI bilayer resist stack.

Au in particular has shown particular promise in producing oriented, size-selected nanowires [3]. While the patterning of Au features onto other III-V materials, such as InP, has been demonstrated down to 50 nm [4], sub-100-nm patterning of Au on GaAs has not been demonstrated, due to the poor adhesion of Au onto GaAs substrates. Because nanowire diameter exhibits a strong dependence on catalyst particle size [5], the smallest-diameter nanowire that can be grown is limited. By using a bilayer-resist process, and through the introduction of a Cr adhesion layer, metal feature sizes under 40 nm were achieved.

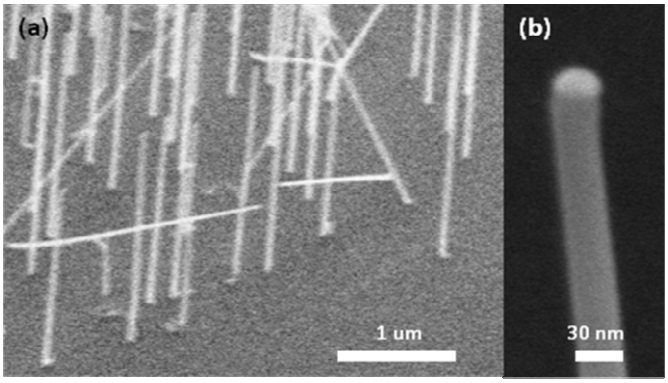

Figure 9: (a) An array of GaAs nanowires grown epitaxially by MOCVD, catalyzed by patterned Au/Cr metal features. (b) A 30-nm-diameter GaAs nanowire, with the metal catalyst clearly visible at the top of the nanowire.

The bilayer-resist structures used had a 50-nm-thick top layer of polymethyl methacrylate (PMMA), and a bottom layer of polymethyl glutarimide (PMGI) with thicknesses between 50nm and 150nm. The PMMA/PMGI resist stack was exposed by electron-beam lithography, then the PMMA and PMGI layers were developed in turn. The PMMA layer was first developed by a cold development process [6], and then a controlled undercut was created in the PMGI layer [7]. A metal stack of Au and Cr was evaporated, with the Cr serving as an adhesion layer. Using a 3-nm-thickness of Cr, we were able to create sub-40-nm metal structures. These structures were subsequently used to grow GaAs nanowires by metal-organic chemical-vapor deposition (MOCVD) with diameters as small as 30 nm.

References:
[1] J. Goldberger, A. I. Hochbaum, R. Fan, and P. Yang, "Silicon vertically integrated nanowire field effect transistors," *Nano Letters*, vol. 46, pp. 973-977 (2006).

[2] X. Duan, Y. Huang, Y. Cui, J. Wang, and C. M. Lieber, "Indium phosphide nanowires as building blocks for nanoscale electronic and optoelectronic devices," *Nature,* vol. 409, pg. 66-69 (2001).

[3] P. Nguyen, H.T. Ng, and M. Meyyappan, "Catalyst Metal Selection for Synthesis of Inorganic Nanowires," *Advanced Materials*, vol. 17, pp. 1773-1777 (2005).

[4] T. Mårtensson, M. Borgström, W. Seifert, B. J. Ohlsson, and L. Samuelson, "Fabrication of individually seeded nanowire arrays by vapor-liquid-solid growth," *Nanotechnology,* vol. 14, pp. 1255-1258 (2003).

[5] Y. Cui, L. J. Lauhon, M. S. Gudiksen, J. Wang, and C. M. Lieber, "Diameter-controlled synthesis of single-crystal silicon nanowires," *Applied Physics Letters*, vol. 78, pp-2214-2216 (2001).

[6] B. Cord, J. Lutkenhaus, and K. K. Berggren, "Optimal temperature for development of poly (methylmethacrylate)," *J. Vac. Sci. Technol. B*, vol. 25, pp. 2013-2016 (2007).

[7] B. Cord, C. Dames, and K. K. Berggren, "Robust shadow-mask evaporation via lithographically controlled undercut," *J. Vac. Sci. Technol. B,* vol. 24, pp. 3139-3143 (2006).

Efficiently Coupling Light to Superconducting Nanowire Single-Photon Detectors

Sponsors:
IARPA

Project Staff:
X. Hu, F. Najafi, F. Marsili, T. Zhong, C. Herder, F. N. C. Wong, K. K. Berggren
Research Laboratory of Electronics, MIT

We developed a superconducting nanowire single-photon detector (SNSPD) system in a close-cycled cryocooler with system detection efficiency (SE) 24.4% and 21.7% at the wavelengths of 1550 nm and 1315 nm, respectively, and a dark count rate ~1000 counts/sec, as shown in Figure 6. This demonstration will enable many applications of SNSPDs such as quantum key distribution, deep-space optical communication and defect-detection for integrated circuits.

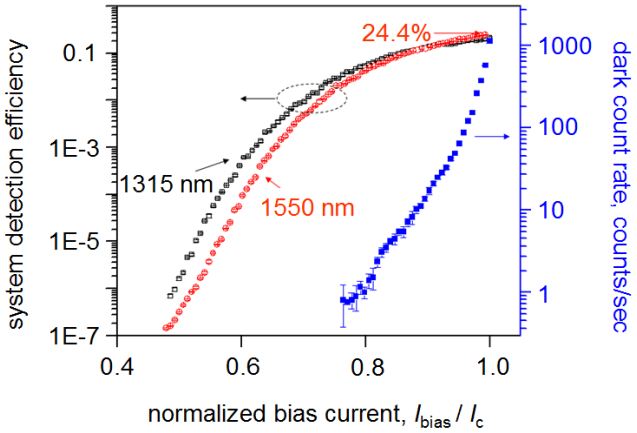

Figure 10: System detection efficiency and dark count rate of a single-photon detector inside a close-cycled cryocooler. The efficiency was measured at the wavelengths of 1315 nm and 1550 nm.

In the past, we successfully developed a robust process to fabricate SNSPDs and demonstrated device detection efficiency (DE) above 50% at near-infrared wavelengths [1]. However, one of its technical challenges is how to efficiently couple light into SNSPDs because of its small active area and its low-temperature operation. To achieve efficient coupling, we fabricated a device with a relatively large area, and, at the same time, a high DE and designed a chip package in a cryocooler. The detector was a circular one with a diameter of 9μm (Figure 7a) integrated with a micro cavity (Figure 7b). We were able to obtain DE ~ 31% (excluding coupling losses) at 1550 nm wavelength. In the chip package (Figure 7c), a fiber-focuser was used to shrink the spot-size of the light from a single-mode fiber down to 5 μm, and the nanopositioners were used to accurately adjust the position of the light spot in-situ three-dimensionally. The detector was directly connected with an SMA connector through wire bonding. The temperature of the chip was cooled down to 2.7 K in the cryocooler.

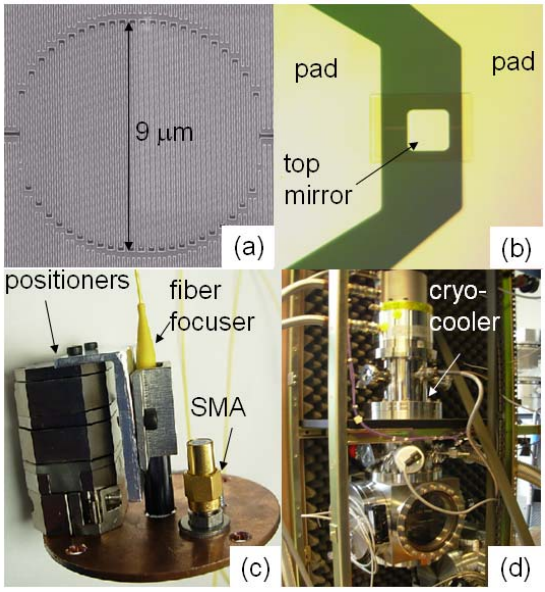

Figure 11: (a) A scanning-electron microscope image of a circular nanowire single-photon detector with a diameter of 9 μm; (b) A top view, optical microscope image of the detector with cavity-integration [1]. (c) The chip package. Note that it is back-illumination, and the chip, aligned with the fiber-focuser, is sitting on the other side of the chip plate. (d) The SNSPD system in a close-cycled cryocooler.

Using this cryogen-free SNSPD system (Figure 7d), we were able to measure the flux and quantum interference of polarization-entangled photons at 1316 nm generated by parametric down conversion in a periodically poled potassium titanyl phosphate (PPKTP) waveguide using this system. We measured 0.8 pairs of polarization-entangled photons per second at a pump power of 96μW and an average two-photon quantum-interference visibility of 97.5% with subtraction of accidentals.

Reference:

[1] K. M. Rosfjord, J. K. W. Yang, E. A. Dauler, A. J. Kerman, V. Anant, B. M. Voronov, G. N. Gol'tsman, and K. K. Berggren, "Nanowire single-photon detector with an integrated optical cavity and anti-reflection coating," *Optics Express*, vol. 14, issue 2, pp. 527-534 (2006).

Low-cost Lloyd's Mirror Interference Lithography

Sponsors:

Singapore-MIT Alliance

Project Staff:

C. Fucetola, H. Korre, K. K. Berggren
Research Laboratory of Electronics, MIT

Interference Lithography (IL) systems generally exist in larger well-equipped laboratories, where their ~50,000 USD price-tag is not a substantial constraint. These tools are designed to pattern periodic structures over large areas (>1mm^2) for applications such as spectroscopy, magnetic storage and nanofabrication process development [1]. However, some of these applications, such as nanofabrication process development, do not require large grating areas. Hence, there also exists a need for < 1 mm^2-area patterning in a variety of smaller labs and educational facilities that is not being met in part due to cost, access, infrastructure, and maintenance requirements of existing IL tools. We have demonstrated a method of IL capable of ~300 nm pitch patterning that uses an extremely low-cost 405 nm diode laser and simplified setup to improve the accessibility of IL to a broader array of laboratories.

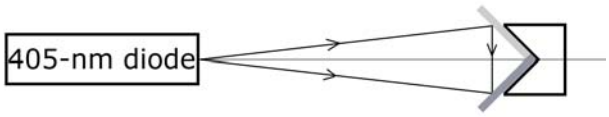

Figure 12: Our Lloyd's mirror lithography system included an inexpensive 405 nm diode laser and an inexpensive mirror/substrate chuck. The mirror/substrate chuck held both a mirror and substrate fixed in a perpendicular orientation

Figure 8 shows our system, which includes a 405-nm GaN diode laser module, a machinist's block, a chrome-coated silicon mirror, substrate and double-sided tape. The laser and the machinist's block were assembled in a linear configuration, and to complete the system, the mirror and substrate were taped to perpendicular surfaces of the machinist's block. During IL exposures, the substrate's photo resist was irradiated with light from both the laser (directly) and mirror (by reflection). Approximately 50 silicon substrates were prepared with a trilayer resist stack to improve the resist profile and facilitate post-lithographic processing. These substrates were exposed and developed and some of them were then imaged in an SEM. One of these substrates is shown in Figure 9.

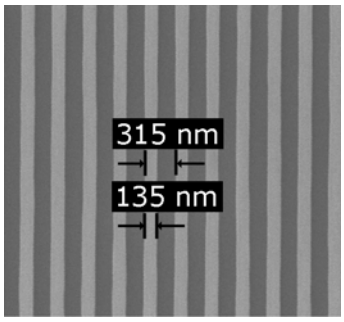

Figure 13: Scanning-Electron Micrograph of diffraction gratings produced by this setup.

In addition to exposures, the associated laser spectrum was measured, enabling calculation of the laser's fringe visibility as it varied along the substrate surface. To compare the exposed resist pattern to the fringe visibility, we measured the first order diffraction efficiency as a function of position along the grating surface. Our measurements indicated that the artifacts seen in both the optical spectrum and resulting grating patterns arose from the laser diode source. Consequently, improving the source characteristics will be the topic of future work.

References:

[1] M. Walsh, "On the design of lithographic interferometers and their application", Ph.D. Thesis, MIT, DSpace.mit.edu (2004).

[2] J. Goodman, Statistical Optics, Wiley, New York, pp. 158-164 (2000).

[3] C. E. Wieman, L. Hollberg, *Rev. Sci. Instrum*. 62, 1, 1-20 (1991).

High resolution surface pattering of fuel cell electrodes

Sponsors:
Alfaisal University and King Abdulaziz City for Science & Technology

Project Staff:
S. Strobel, C. Kirkendall, K. K. Berggren
Research Laboratory of Electronics, MIT

Fuel cells are a competitive candidate for powering ecologically sound transportation and reducing environmental pollution. They produce green electrical energy via conversion of chemical reactants, e.g. hydrogen and oxygen into water. A fuel cell consists of a semipermeable membrane (electrolyte) sandwiched between two electrodes, each coated with a reaction enhancing catalyst layer (Figure 10a). In proton exchange membrane fuel cells (PEMFCs), the hydrogen splits at the anode into protons and electrons. The protons diffuse through the membrane, while the electrons are passed through the load. At the cathode, electrons, protons, and oxygen react at the catalyst to form pure water, the sole product of a hydrogen-oxygen fuel cell. Chemical reactions within a fuel cell only occur at the location where the fuel, electrolyte, and catalyst meet, also referred to the triple phase boundary (TPB). Thus, the size of this interface largely determines the efficiency of a fuel cell.

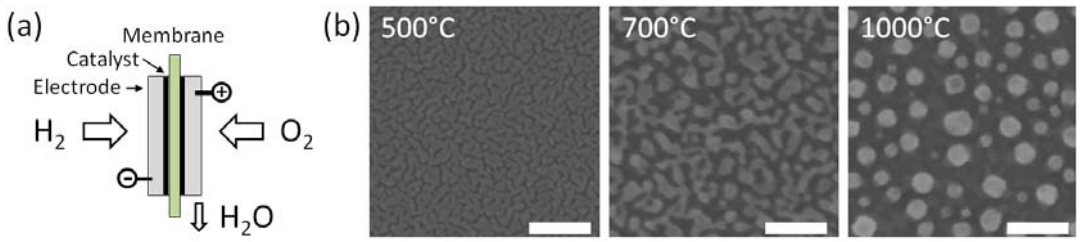

Figure 14: (a) Schematic of a fuel cell. Hydrogen and oxygen are converted into electricity and water. (b) Platinum thin film (3 nm) thermally dewetted for 30s at temperatures of 500°, 700°, and 1000°C, respectively. (scale bar: 100 nm)

Our project focuses to increase these TPBs by nano-structuring the electrodes using two methods. One attempt uses high resolution electron-beam lithography patterning, whereas the other takes advantage of the thermal dewetting phenomena in platinum thin films. By heating a metal thin film, reorganization may occur. Depending on the dewetting-parameters, either a perforated, mesh-like, or even dot-like structure may result. Systematic investigations of dewetting parameters including platinum layer thickness, annealing-temperature, and annealing-time were performed. SEM images reveal that structure dimensions down to 10nm can be achieved with this technique. Figure 10b shows a sequence of samples with a 3nm platinum layer dewetted for 30sec, each at a different temperature. As the temperature is increased, a clear transition from a perforated layer to detached dots occurs.

References:

[1] A. M. Higgins, and R. A. L. Jones, "Anisotropic spinodal dewetting as a route to self-assembly of patterned surfaces", *Nature* 404: 476-478 (2000).

[2] R. Xie, A. Karim, J. F. Douglas, C. C. Han, and R. A. Weiss1, "Spinodal Dewetting of Thin Polymer Films", *Phys Rev Lett.* 81(6): 1251-1254 (1998).

Sub-15-nm pattern transfer and nanoimprint molds

Sponsors:

Alfaisal University and King Abdulaziz City for Science & Technology

Project Staff:

D. Morecroft, J. K. W. Yang, S. Schuster, K. K. Berggren
Research Laboratory of Electronics, MIT

Q. Xia, W. Wu, R. S. Williams
Hewlett-Packard Laboratories

Nanoimprint lithography is capable of high-throughput, low cost and high resolution, but it relies on other techniques, such as molecular beam epitaxy (MBE) followed by selective wet etching, to fabricate sub-10-nm molds [1]. These techniques are typically limited in flexibility of pattern design, permitting, for example, only simple periodic linear patterns to be formed. Electron-beam lithography (EBL), on the other hand, is capable of arbitrary pattern design, but the ultimate feature density is generally limited by proximity effects. Thus, it remains a challenge to fabricate sub-30-nm arbitrary-pattern nanoimprint molds. We have addressed this challenge by using an optimized process with EBL and reactive ion etching (RIE).

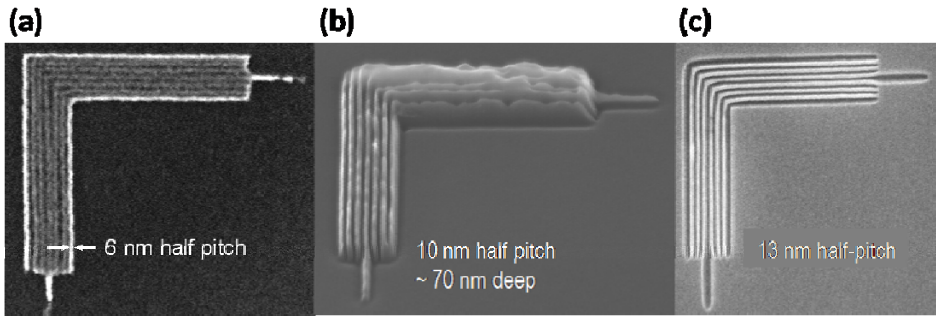

Figure 15: Scanning electron microscopy images of nested L patterns (a) in negative tone resist using electron beam lithography, (b) pattern transferred into silicon using reactive ion etching and (c) imprinted into resist using UV-cure nanoimprint lithography.

Previously results have shown that negative tone resist can be used in combination with a salty developer technique to enhance contrast. Using this technique sub-15-nm nested L patterns were written in hydrogen silsesquioxane (HSQ) resist using a Raith 150^{TWO} tool, as shown in Figure 11a. Combining the electron beam lithography with RIE offers the possibility for high resolution with high aspect ratio structures to facilitate nanoimprint into the resist and subsequent pattern transfer. Figure 11b shows a tilted microscopy image of one of the nested L structures transferred into the silicon substrate with a hydrogen bromide (HBr) plasma. The HBr plasma shows excellent selectivity between the HSQ and silicon substrate. UV-cure nanoimprint was carried out in the Quantum Science Research Group (QSR) at Hewlett-Packard Laboratory. Figure 11c shows that successful nanoimprint was carried out into the nanoimprint resist. An organic release layer was deposited on the mold prior to the imprint using atomic layer deposition. The results show that dense pattern arrays with sub-10 nm feature sizes can be imprinted with high fidelity.

There are many potential applications for this patterning process, for example nanopatterned electrodes for fuel cells and batteries where the increased surface area may enhance the catalytic activity.

References:

[1] M. D. Austin, W. Zhang, H. Ge, D. Wasserman, S. A. Lyon, S. Y. Chou, "6 nm half-pitch lines and 0.04μm^2 static random access memory patterns by nanoimprint lithography", *Nanotechnology* 16, 1058 (2005).

[2] J. K. W. Yang and K. K. Berggren, "Using High Contrast Salty Development of Hydrogen Silsesquioxane for Sub-10 nm Half Pitch Lithography", *J. Vac. Sci. Technol. B*, vol. 25(6), pp. 2025 (2007).

Superconducting hybrid ion traps for molecular quantum computing

Sponsors:
NSF Center for Ultracold Atoms, DARPA, MIT

Project Staff:
S. A. Schulz, A. McCaughan, P. Antohi, Y. Ge, I. Chuang, K. K. Berggren
Research Laboratory of Electronics, MIT

Schemes for quantum computing based on nuclear magnetic resonance techniques [1, 2], ion trapping [3] and solid state techniques [4] have demonstrated basic quantum algorithms. The scalability regarding more complex quantum algorithms needs physical systems with longer

coherence times and enhanced control of multiple qubits at the same time. A new approach for building scalable systems for ion based quantum computing is the combination of a planar Paul microtrap [5] in a cryogenic environment [6] with a superconducting microwave cavity [7, 8]. Single polar molecular ions will be trapped above the superconducting planar trap and their rotational states will be used as qubit levels. The integrated microwave resonator will allow coherent qubit control and the cavity coupling of the microwave photons is used for the quantum bus.

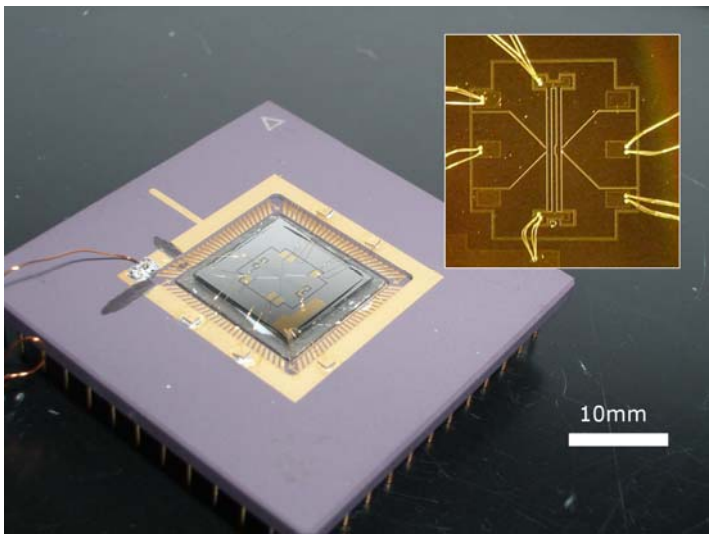

Figure 16: Superconducting linear Paul trap fabricated by Nb sputtering and lithography. The ion trap chip is operated in a cryogenic environment at 6K. The inset shows the trap geometry from top view [10].

The hybridization of the quantum system is based on an electrical interface of a quantum memory (polar molecular ions) and a quantum bus (microwave cavity) [9]. The integration of the microwave stripline resonator in the superconducting ion trap will provide a low heating rate of the molecular ions [7] in combination with a large quality factor for fast gate operations using the microwave cavity [6].

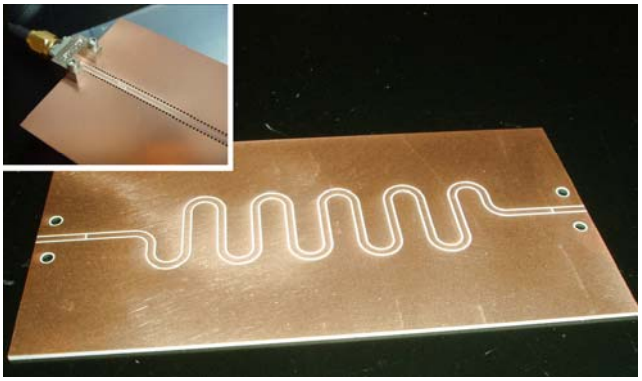

Figure 17: Printed circuit resonators for test measurements in the GHz frequency range.

The superconducting microwave cavity is simulated numerically and fabricated out of Nb/NbN, and will be integrated in an existing superconducting Nb/NbN ion trap. The existing cryogenic cooled 100 micrometer-scaled surface trap (Figure 12) showed a heating rate of 10 to 20 vibrational quanta per second [10]. The superconducting layer thickness was about 0.14mm. The superconducting microwave resonator will be implemented in a specific linear ion trap geometry, and unloaded quality factors on the order of 10000 to 100000 are expected. In intial tests with

printed circuit board resonators (Figure 12), the properties of the resonators will be investigated. After this, the design will be downscaled to Nb/NbN based microwave resonators fabricated using microlithography techniques.

References:

[1] I. L. Chuang, L. M. K. Vandersypen, X. Zhou, D. W. Leung, and S. Lloyd, "Experimental realization of a quantum algorithm," *Nature* 393, 143 (1998).

[2] J. A. Jones, M. Mosca, and R. H. Hansen, "Implementation of a quantum search algorithm on a quantum computer," *Nature* 393, 344 (1998).

[3] S. Gulde, M. Riebe, G. P. T. Lancaster, Becher, J. Eschner, F. Schmidt-Kaler, I. L. Chuang, and R. Blatt, "Implementation of the Deutsch Jozsa algorithm on an ion trap Quantum computer," *Nature* 421, 48 (2003).

[4] L. DiCarlo, J. M. Chow, J. M. Gambetta, L. S. Bishop, B. R. Johnson, D. I. Schuster, J. Majer, A. Blais, L. Frunzio, S. M. Girvin, and R. J. Schoelkopf, "Demonstration of two qubit algorithms with a superconducting quantum processor," *Nature* 08121 (2009).

[5] D. Stick, W. K. Hensinger, S. Olmschenk, M. J. Madsen, K. Schwab, and C. Monroe, "Ion trap in a semiconductor chip," *Nature Physics* 2, 36 (2006).

[6] J. Labaziewcz, Y. Ge, P. Antohi, D. Leibrandt, K. Brown, and I. L. Chuang, "Suppression of Heating Rates in Cryogenic Surface Electrode Ion traps," *Phys. Rev. Lett.* 100, 013001 (2008).

[7] A. André, D. DeMille, J. M. Doyle, M. D. Lukin, S. E. Maxwell, P. Rabl, R. J. Schoelkopf, and P. Zoller, "A coherent all electrical interface between polar molecules and mesoscopic superconducting resonators," *Nature* 2, 636 (2006).

[8] K. Tordrup, and K. Molmer, "Quantum computing with a single molecular ensemble and a Cooper pair box," *Phys. Rev. A* 77, 020301 (2008).

[9] D. I. Schuster, L. S. Bishop, I. L. Chuang, D. DeMille, and R. J. Schoelkopf, "Cavity QED in a molecular ion trap," *arXiv:0903.3552* (2009).

[10] Y. Ge, E. Dauler, J. Labaziewicz, S. Wang, I. Chuang, K. K. Berggren, unpublished (2008).

Scanning-Electron-Beam Lithography (SEBL) Facility

Sponsors:
MIT Institute Facility under RLE

Project Staff:
M. K. Mondol, F. Zhang, H. I. Smith, K. K. Berggren
Research Laboratory of Electronics, MIT

In 2004, the Nanostructures Lab converted its scanning-electron-beam-lithography (SEBL) facility in Room 38-165 into an Institute-wide service facility under the Research Laboratory of Electronics (RLE). This facility provides MIT and outside users with easily accessible e-beam lithography, coupled with resident expertise and advice. The facility is managed by Mark Mondol who provides training on the e-beam tools, direct patterning service, and advice on optimal nanofabrication techniques and strategies. The NanoStructures Laboratory (NSL) and the

Microsystems Technology Laboratories (MTL) have service facilities for spin coating of resists, resist development and other forms of processing.

Projects that made use of the SEBL facility during the past year included: patterned nanotube growth; relief templates for self assembly of block copolymers; point-contact devices; 1-D and 2-D photonic crystals; ring-resonator add/drop filters; optical-polarization splitter-rotator devices; novel liquid-crystal devices; magnetic-memory devices; quantum photodetectors; templates for nanoimprint lithography; photomasks for interferometric-spatial-phase-imaging alignment and gapping; 4-point contacts for measurements on nanotubes and nanowires; III-V compound T-gate HEMTs and arrays of Fresnel zone plates. Research in lithographic processing included extreme cold development of PMMA and novel developer solutions for HSQ which demonstrated improved resolution and contrast. Use of the facility, by the MIT community, was widespread, there were: 25 Principal Investigators, 7 Departments, 8 Labs or Centers, 2 non-MIT entities and 45 distinct trained users over the last year.

Two SEBL tools are available. The Raith Turnkey 150 system is shown in Figure 13. Its electron-optical column is essentially identical to that of a Zeiss Gemini SEM, and provides a beam diameter as fine as 2 nm. Linewidths of ≤ 9 nm have been written with the system, as illustrated in Figure 14. The Raith 150 includes a pattern generator and laser-interferometer-controlled stage with an integrated software package which was upgraded to version 4.0 in the past year. This upgrade improved writing speed and system stability. Version 4.0 software now allows users to do automated field alignment to approximately ± 25nm. The system can operate from 1 to 30keV accelerating voltage. Wafers up to 150 mm can be loaded into the system. Typically, users are trained for 3 to 10 hours and then allowed to operate the tool on their own. The tool is available, for most users, 24 hours a day, 7 days a week.

Figure 15 is a photograph of the VS-26 system. This instrument was put together at MIT from two systems (VS-2A and VS-6) obtained as gifts from IBM in the mid 1990's. VS-26 has a minimum beam diameter of about 10 nm. It operates at a fixed accelerating voltage of 50keV. Conversion software has been developed which allows a CAD data file to be fractured and translated prior to exposure, additional software was developed to generate arbitrary arcs. Substrates up to 200 mm diameter can be exposed at linewidths down to ~30 nm. However, the area available for patterning is limited to 95x95 mm.

The Raith 150 is used in a program to develop spatial-phase-locked e-beam lithography, described elsewhere. The objectives of that program are to achieve sub-1 nm pattern-placement accuracy, and to reduce the cost and complexity of SEBL. In a conventional SEBL system costing several million dollars, pattern placement accuracy is typically much worse than 10 nm.
The SEBL facility encourages users with a variety of experience levels and requirements. Experienced users are able to carry out complex, multilevel aligned exposures on the Raith-150 tool. Less experienced users get hands-on instructions from facility staff, and guidance during the learning and initial fabrication stages.

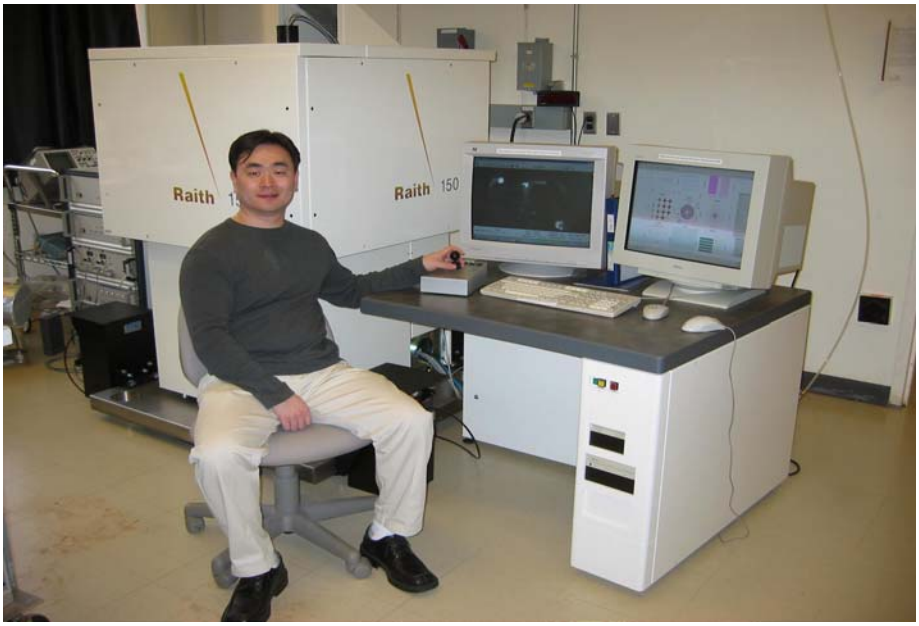

Figure 13: The Raith-150 electron-beam lithography system. This tool provides sub-20-nm patterning resolution, and pattern-placement accuracy ~1nm via spatial phase locking. The operator is Dr. Feng Zhang.

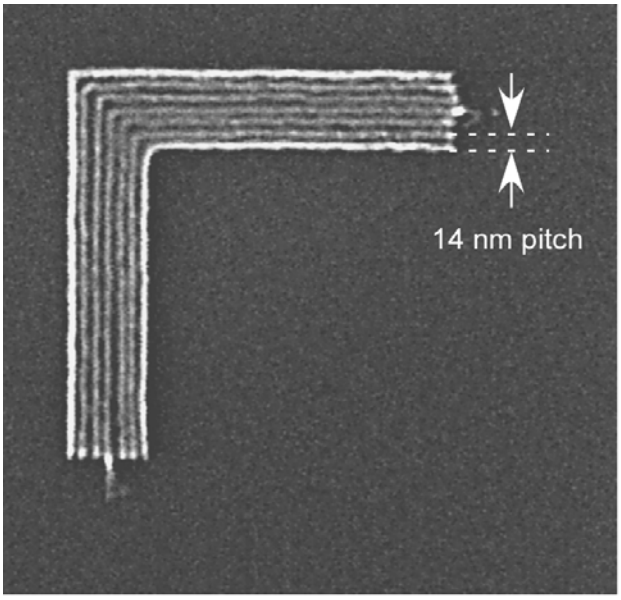

Figure 14: Scanning-electron micrograph of exposed and developed HSQ illustrating the resolution of the Raith 150 SEBL system. (J. K. W. Yang and K. K. Berggren, "Using High-Contrast Salty Development of Hydrogen Silsesquioxane for Sub-10-nm-Half-Pitch Lithography," Journal of Vacuum Science & Technology B, submitted for publication (2007)

Figure 15: Photograph of the VS-26 scanning-electron-beam lithography system.

Publications

Journal Articles, Published

M. Ahn, R. K. Heilmann, and M. L. Schattenburg, “Fabrication of 200 Nm Period Blazed Transmission Gratings on Silicon-on-insulator Wafers,” Journal of Vacuum Science and Technology B, Vol. 26, pp. 2179-2182, 2008.

R. Amatya, C. W. Holzwarth, H. I. Smith, and R. J. Ram, “Precision Tunable Silicon Compatible Microring Filters,” IEEE Photonics Technology Letters, Vol. 20, 2008.

V. Anant, A. J. Kerman, E. A. Dauler, J. K. W. Yang, K. M. Rosfjord, and K. K. Berggren, “Optical Properties of Superconducting Nanowire Single-Photon Detectors,” Optics Express, vol. 16, pp. 10750-10761, 3 July 2008.

T. L. Andrew, H.-Y. Tsai, and R. Menon, "Confining light to deep sub-wavelength dimensions to enable optical nanopatterning," Science, Vol. 324, pp. 917-921, 2009.

T. Barwicz, C. W. Holzwarth, P. T. Rakich, M. A. Popovi, E. P. Ippen, and H. I. Smith, “Optical Loss in Silicon Microphotonic Waveguides Induced by Metallic Contamination,” Applied Physics Letters, vol. 92, p. 131108, 2008.

D. M. Berns, M. S. Rudner, S. O. Valenzuela, K. K. Berggren, W. D. Oliver, L. S. Levitov, and T. P. Orlando, “Amplitude Spectroscopy of a Solid-State Artificial Atom,” Nature, vol. 455, pp. 51-57, 4 September 2008.

I. Bita, J. K. W. Yang, Y.-S. Jung, C. A. Ross, E. L. Thomas, and K. K. Berggren, “Graphoepitaxy of Self-Assembled Block Copolymers on Two-Dimensional Periodic Patterned Templates,” Science, vol. 321, pp. 939-943, 15 August 2008.

C. H. Chang, R. K. Heilmann, M. L. Schattenburg, and P. Glenn, “Design of a Double-Pass Shear Mode Acousto-optical Modulator,” Review of Scientific Instruments, Vol. 79, pp. 033104-1-5, 2008.

C. H. Chang, Y. Zhao, R. K. Heilmann, and M. L. Schattenburg, “Fabrication of 50 Nm-period Gratings with Multilevel Interference Lithography,” Optics Letters, Vol. 33, pp. 1572-1574, 2008.

C. H. Chang, Y. Zhao, R. K. Heilmann, and M. L. Schattenburg, “Spatial-frequency Multiplication with Multilayer Interference Lithography,” Journal of Vacuum Science and Technology B, Vol. 26, pp. 2135-2138, 2008.

V. P. Chuang, C. A. Ross, P. Bilalis, and N. Hadjichristidis , “Nanoscale Rings Fabricated Using Self-Assembled Triblock Terpolymer Templates,” ACS Nano, Vol. 2, pp. 2007-2014, 2008.

V. P. Chuang, C. A. Ross, J. Gwyther, and I. Manners , “Self-Assembled Nanoscale Ring Arrays from a Polystyrene-b-polyferrocenylsilane-b-poly(2-vinylpyridine) Triblock Terpolymer Thin Film,” Advanced Materials, Vol. 21, pp. 1-5, 2009.

Dauler, E.A., A.J. Kerman, B.S. Robinson, J.K.W. Yang, B. Voronov, G. Gol'tsman, S.A. Hamilton, and K.K. Berggren, “Photon-Number-Resolution with Sub-30-ps Timing using Multi-Element Superconducting Nanowire Single Photon Detectors,” Journal of Modern Optics, Vol. 56, No. 2 & 3. (January 2009), pp. 364-373.

E. A. Dauler, M. J. Stevens, B. Baek, R. Molnar, S. A. Hamilton, R. P. Mirin, S.-W. Nam, and K. K. Berggren, “Measuring intensity correlations with a two-element superconducting nanowire single photon detector,” Physical Review A, vol. 78, 2008.

P. Hashemi, M. Canonico, J. K. W. Yang, L. Gomez, K. K. Berggren, and J. L. Hoyt, “Fabrication and Characterization of Suspended Uniaxial Tensile Strained-Si Nanowires for Gate-All-Around n-MOSFETs,” ECS (Electrochemical Society) Transactions, vol. 16, pp. 57-68, October 2008.

R. K. Heilmann, M. Ahn, E. M. Gullikson, and M. L. Schattenburg, “Blazed High-Efficiency X-ray Diffraction via Transmission through Arrays of Nanometer-scale Mirrors,” Optics Express, Vol. 16, pp. 8658-8669, 2008.

C. W. Holzwarth, R. Amatya, M. Dahlem, A. Khilo, F. X. Kärtner, E. P.

Ippen, R. J. Ram, and H. I. Smith, “Fabrication Strategies for Filter Banks based on

Microring Resonators,” Journal of Vacuum Science and Technology B, Vol. 26, pp. 2164-2167, 2008.

Y. S. Jung, W. Jung and C. A. Ross, “Nanofabricated Concentric Ring Structures by Templated Self-Assembly of a Diblock Copolymer,” Nano Letters, Vol. 8, pp 2975–2981, 2008.

Y. S. Jung†, W. Jung†, H. L. Tuller and C. A. Ross, “Nanowire Conductive Polymer Gas Sensor Patterned Using Self-Assembled Block Copolymer Lithography,” Nano Letters, Vol. 8, pp 3776–3780, 2008.

Y. S. Jung and C. A. Ross, “Well-Ordered Thin-Film Nanopore Arrays Formed Using a Block-Copolymer Template”, Small, to be published, 2009.

Y. S. Jung and C. A. Ross, “Solvent-Vapor-Induced Tunability of Self-Assembled Block Copolymer Patterns”, Advanced Materials, to be published, 2009.

R. Menon, P. Rogge, and H.-Y. Tsai, "Design of diffractive lenses that generate optical nulls without phase singularities," Journal of the Optical Society of America A, Vol. 26, pp. 297-304, 2009.

E. E. Moon and H. I. Smith, "Nanometer-level Alignment to a Substrate-embedded Coordinate System," Journal of Vacuum Science and Technology B, Vol. 26, p. 2341, 2008.

C. Nam, B. G. Ng, F. J. Castaño, M. D. Mascaro, and C. A. Ross, “Current-driven Vortex Formation in a Magnetic Multilayer Ring,” Applied Physics Letters, Vol. 94, 2009.

C. Nam, B. G. Ng, F. J. Castaño, and C. A. Ross, “Effect of Magnetic Field Direction on the Remanent Resistance Levels and Vortex Chirality of a Multilayered Magnetic Ring,” Journal of Applied Physics, Vol. 105, pp. 033918-1-4, 2009.

T. B. O'Reilly and H. I. Smith, “Linewidth Uniformity in Lloyd's Mirror Interference Lithography Systems,” Journal of Vacuum Science and Technology B, Vol. 26, p. 2131, 2008.

T. Reisinger, A.A. Patel, H. Reingruber, K. Fladischer, W.E. Ernst, G. Bracco, H.I.Smith, and B. Holst, "Poisson's splot with molecules," Physical Review A, Vol. 79,pp.053823-1:4, 2009.

C. A., Ross, Y. S. Jung, V. P.Chuang, F. Ilievski, J. K. W. Yang, I. Bita, E. L. Thomas, H. I. Smith, K. K. Berggren, J. G.Vansco, and J. Y. Cheng, “Si-Containing Block Copolymers for Self-Assembled Nanolithography (invited),” Journal of Vacuum Science and Technology B, vol. 26, pp. 2489-2494, 2008.

V. Sharma, Q. Yan, C.C. Wong, W. C. Carter and Y.-M. Chiang, "Controlled and rapid ordering of oppositely charged colloidal particles," Journal of Colloid and Interface Science, Vol. 333, pp. 230-236, 2009.

T. Shih, A. Kurs, M. Dahlem, G. Petrich, M. Soljačić, E. Ippen, L. Kolodziejski, K. Hall, and M. Kesler, “Supercollimation in Photonic Crystals Composed of Silicon Rods,” Applied Physics Letters, Vol. 93, 2008.

J. Sun, C. W. Holzwarth, M. Dahlem, J. T. Hastings, and H. I. Smith, "Accurate Frequency Alignment in Fabrication of High-order Microring-resonator Filters,” Optics Express, Vol. 16, pp. 15958-15963, 2008.

H.-Y. Tsai, H. I. Smith, and R. Menon, "Reduction of focal-spot size using dichromats in absorbance modulation," Optics Letters, Vol. 33, pp. 2916-2918, 2008.

W. Wu, W. M. Tong, J. Bartman, Y. Chen, R. Walmsley, Z. Yu, Q. Xia, I. Park, C. Picciotto, J. Gao, S.-Y. Wang, D. Morecroft, J. K. W. Yang, K. K. Berggren, and R. S. Williams, “Sub-10 nm Nanoimprint Lithography by Wafer Bowing,” Nano Letters, 10.1021/nl802295n, 5 pages, published on web 7 October, 2008.

Theses

X. -L. Hu, “Coupling Light to Superconductive Photon Counters,” M.S. Thesis, Department of EECS, May 2008.

J. Leu, “ Templated Self-Assembly of Sub-10-nm Quantum Dots,” M.S. Thesis, Department of EECS, May 2008.

L. Battistella, “Directed Self-Assembly of Colloidal Nanoparticles by Sub-10 nm Templates,” M.S. Thesis, Politecnico di Torino, September 2009.

E. Dauler, “Multi-Element Superconducting Nanowire Single Photon Detectors,” Ph.D. Thesis, Department of EECS, January 2009.

J. K. W. Yang, “Superconducting Nanowire Single-Photon Detectors and Sub-10-nm Lithography,” Ph.D. Thesis, Department of EECS, April 2009.

B. Cord, “Sub-10-nm Patterning with Charged-Particle Lithography”, Ph.D. Thesis, Department of EECS, May 2009.

C. W. Holzwarth, “Material Selection and Nanofabrication Techniques for Electronic Photonic Integrated Circuits,” Ph.D. Thesis, Department of Materials Science and Engineering, June 2009.

V. Chuang, “Fabrication and Characterization of Novel Nanostructures Based on Block Copolymer Lithography,” Ph.D. Thesis, Department of Materials Science and Engineering, July 2009.

V. Sharma, “Novel Methods of Making Non-Close-Packed Structures from Colloidal Self-Assembly,” Ph.D. Thesis, Department of Materials Science and Engineering, September 2009.

Patents

E. E. Moon, “Nanometer-level mix-and-match scanning tip and electron beam lithography using global backside position reference marks”, US Patent # 7,535,581, date of issue May 19, 2009.

V. Sharma, W. C. Carter, and Y.-M. Chiang, "Ordered colloidal structures and methods of preparation," US Patent Application 61/146,282, filed January 21, 2009.

E. E. Moon, “Nanometer-precision tip-to-substrate control and pattern registration for scanning-probe lithography”, US Patent # 7,474,410, date of issue January 6, 2009.

R. Menon, T. L. Andrew and F. Stellacci, “Optical 3-D nanopatterning using multi-color saturable transitions,” Technology disclosure submitted December 2008.

R. Menon, “Ultra-high efficiency multi-junction solar cells using polychromatic diffractive concentrators,” US Patent application filed October 17, 2008.

R. Menon, “Superresolution imaging using multiple wavelengths,” US Patent application filed October 17, 2008.

R.Menon, P. Rogge, and H-Y. Tsai, “Multiple-wavelength, binary diffractive lenses,” US Patent application filed October 17, 2008.

R. Menon, and H. I. Smith, “Nanoscale imaging via absorbance modulation,” Patent application filed August 2008.

I. Bita, E. L. Thomas, J. K. W. Yang, Y. S. Jung, C. A. Ross, and K. K. Berggren, “Self-assembly technique applicable to large areas and nanofabrication,” U.S. Patent Application No., 12/239362, September 26, 2008.

R. Menon and H. I. Smith, “Imaging system and method employing beam folding,” US 7,405,806, June 29, 2008.